ORIGINAL

THE OHIO STATE UNIVERSITY
Research Foundation
1314 Kinnear Road
Columbus, OH 43212-1194

DE-FG02-87ER13749

DOE/ER/13749--2

DE90 012868

RESEARCH PROPOSAL RENEWAL

Submitted To

U.S. Department of Energy
Division of Materials Sciences
Office of Basic Energy Sciences
Washington, D.C. 20545

Submitted By

Laszlo Adler
Principal Investigator

Nondestructive Evaluation Group
The Ohio State University
Department of Welding Engineering
Columbus, Ohio 43210

Entitled

INVESTIGATION OF ULTRASONIC WAVE INTERACTIONS WITH FLUID-SATURATED POROUS ROCKS

Institutional Approval:

Richard L. Wright
Vice President for
Development
The Ohio State University
Research Foundation
(614) 292-4283

OFFICIAL FILE COPY

DISCLAIMER

TABLE OF CONTENTS

	Page
SUMMARY	1
Previous Results	1
Proposed Research	3
I. PROGRESS REPORT	5
1 Surface Wave Techniques	5
1.1 Corrugated Surface Technique	7
1.2 Direct Excitation Technique	12
2 Reflection and Transmission of Elastic Waves at Boundaries Between Fluid and Fluid-Saturated Porous Solids	21
2.1 Introduction	21
2.2 Theory	23
2.3 Numerical Results	24
2.4 Experimental Results	30
3 Interaction of Ultrasonic Waves With Thin Fluid-Saturated Porous Plates: Theory and Application of Lamb Wave Technique	37
3.1 Introduction	37
3.2 Theoretical Analysis	39
3.2.1 Field Solution	39
3.2.2 Slow Wave Influence on Dispersion Curve	41
3.2.3 Experimental Procedure	43
3.2.4 Sample Description	46
3.3 Results and Discussion	50
3.3.1 Results on Synthetic Porous Plates	50
3.3.2 Results on Natural Porous Plates	52
3.3.3 Comparison of Bulk and Lamb Wave Techniques	56
4 Slow Wave Propagation in Air-Filled Porous Materials	58
4.1 Introduction	58
4.2 Theoretical Considerations	60
4.3 Experimental Arrangement and Results	65

II. PROPOSED RESEARCH 76

1 Surface Wave Technique 78

2 Lamb Wave Technique 80

3 Air-Saturation Technique 82

REFERENCES 84

PUBLICATIONS 86

PERSONNEL 88

CURRENT SUPPORT 89

BUDGET 90

SUMMARY

PREVIOUS RESULTS

During the past three years we conducted an investigation of ultrasonic surface waves and bulk waves with fluid-filled porous materials. First, we concentrated on the propagation of various surface waves on fluid-saturated porous materials, both synthetic and natural rocks. We developed two novel techniques for surface wave studies. In order to extend our surface wave studies to other guided wave modes, we formulated the general problem of reflection and transmission of elastic waves through various interfaces of fluid-filled porous materials. We carried out numerical calculations and verified, by experiment, the angular behavior of the reflection and transmission coefficients for both fast and slow waves, as well as for shear waves. We have shown that although the boundary conditions affect the strength of the transmitted slow waves through the porous materials, a more major role is played by volumetric attenuation. To increase the detectability of slow waves we introduced another new method based on the generation and detection of leaky Lamb waves. We have shown, both experimentally and theoretically, that the lowest Lamb mode is due to the slow wave component in the porous material. This Lamb wave technique shows superior sensitivity compared to the more conventional bulk technique. We developed a new technique based on the transmission of airborne ultrasonic waves through air-saturated porous plates in order to observe slow waves in natural rocks. To the best of

our knowledge, our preliminary results represent the first irrefutable evidence of slow waves in fluid-saturated natural rocks, such as different types of sandstones. About 12 papers have been published on the subject of this work supported by DOE. Our main achievements for the last three years, which also serve as the background for our renewal proposal, are briefly summarized in the first part of this program and are highlighted in the Table of Contents.

PROPOSED RESEARCH

Objectives of Proposed Research

During the next three years of this proposed work we plan to continue our investigation of ultrasonic waves, especially the slow compressional wave, with fluid-saturated porous solids, especially rocks. This research effort should find applications in the geophysical evaluation of fluid-bearing porous rocks where parameters such as tortuosity, permeability, saturation level, and internal impurities are difficult to measure by conventional techniques.

Summary of Proposed Research

The proposed investigation of ultrasonic wave interaction with fluid-saturated porous materials may be divided into three major subtasks:

1. Experimental study of surface wave propagation on fluid-saturated porous materials. A new, so-called direct excitation technique will be used on both air- and water-saturated samples.
2. Further development of the Lamb wave technique recently introduced to study guided wave propagation in thin fluid-saturated porous plates. The analytical treatment will be extended to account for viscous losses and scattering inhomogeneities.
3. Theoretical and experimental study of slow wave propagation in fluid-saturated natural rocks. A new technique based on the transmission of airborne ultrasound through air-saturated porous plates will be

used to determine otherwise inaccessible material properties such as tortuosity, permeability, internal friction caused by impurities, etc.

I. PROGRESS REPORT

1 SURFACE WAVE TECHNIQUES

Generally, two types of interface modes can propagate along the surface of a solid sample immersed in fluid: there is a true mode called Stoneley wave and a pseudo-mode called leaky Rayleigh wave. The true mode has a phase velocity lower than all the bulk velocities in the two media and produces evanescent fields only in the solid and the liquid as it propagates along the interface. Since the energy of this mode is strictly confined to the interface region, its generation and detection presents a difficult technical problem. On the other hand, the leaky Rayleigh mode has a phase velocity higher than the sound velocity in the liquid, therefore it leaks its energy into the liquid as it propagates along the interface. This mode can be easily generated and detected by the phase-matching compressional wave in the liquid at the so-called Rayleigh angle, at least whenever this angle is not higher than approximately 60°. It should be mentioned that this mode becomes nonpropagatory whenever the shear velocity in the solid is lower than the sound velocity in the fluid, which is true for many natural rocks.

Feng and Johnson showed that a maximum of three different types of surface modes can exist on a fluid/fluid-saturated porous solid interface depending on the shear velocity of the frame and the surface conditions, i.e. whether the pores are open or closed

[1]. However, in many natural rocks with shear velocities lower than the sound velocity in water and open pores at the surface, there is but one principal surface mode, namely the Stoneley mode, which becomes leaky into the slow wave when its velocity is higher, i.e. in most cases of interest to us.

1.1 Corrugated Surface Technique

One way to generate both Rayleigh- and Stoneley-type surface modes on a liquid-solid interface is to make the surface slightly corrugated so that these modes become leaky into both media at particular frequencies where the periodicity of the corrugation is an integer multiple of the surface wavelength. These resonances produce sharp minima in the reflection coefficient of the interface, which can be used to calculate the surface wave velocities [2,3]. The advantage of this technique over the conventional Rayleigh angle method is that it can be used to generate surface modes of very low phase velocities which do not leak (or only at a very high angle) as they propagate along a smooth liquid-solid interface. We have adapted this technique to study surface wave propagation on fluid-saturated porous materials [4].

Figure 1 shows the deconvolved spectrum of the backscattered signal from the corrugated surface of a water-saturated porous cemented glass bead specimen. Three distinct minima can be observed on this reflection spectrum. Since the shear velocity (1410 m/s) is lower than the sound velocity in water, the leaky Rayleigh mode is nonpropagatory. The highest (third) minimum at 2.3 MHz corresponds to the compressional wave in water propagating at 1460 m/s. The middle (second) miminum at 1.8 MHz corresponds to a Stoneley-type interface mode of 1140 m/s velocity, which is slightly leaky into the slow compressional mode. Finally, the lowest (1st) minimum at 1.3 MHz corresponds to a wave propagating at 825 m/s velocity. Although this value is very close to the velocity of the new true surface mode predicted by Feng and Johnson

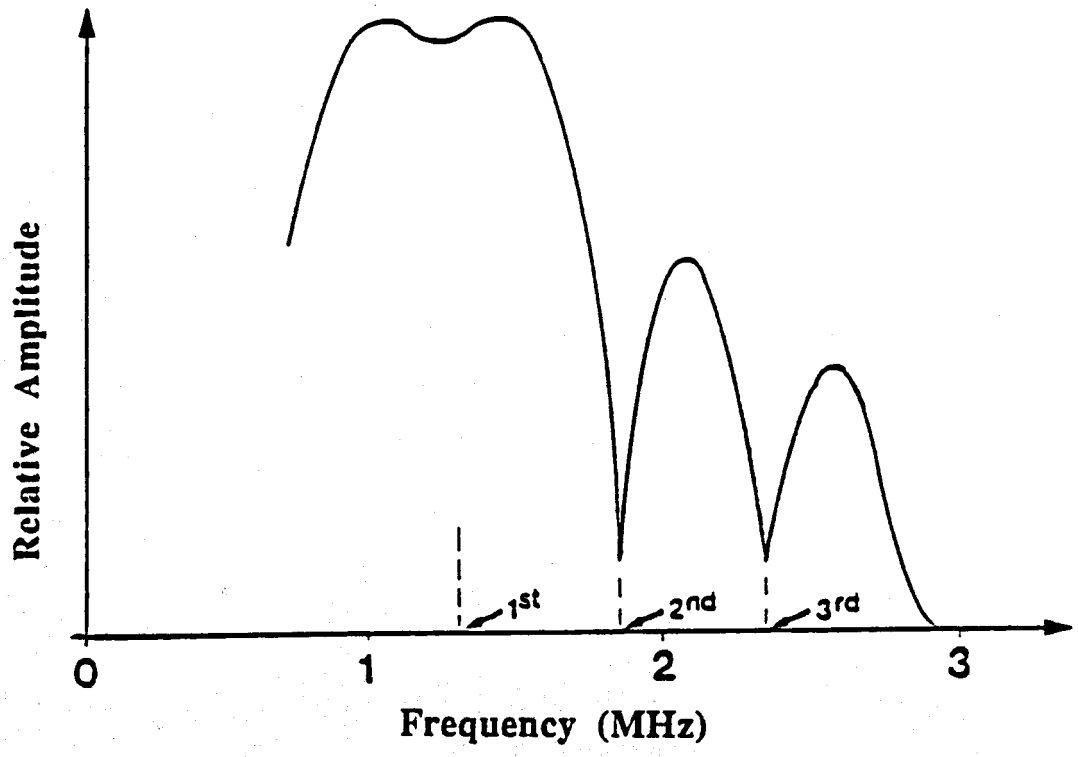

Fig. 1. Deconvolved spectrum of the backscattered signal from a water-saturated porous solid (grade 15, cemented glass beads) periodic interface, period = 635 μm, depth = 320 μm.

for the case of closed pores at the surface [1], we found that the pores were actually quite open due to the machining technique, therefore this minimum is probably caused by the slow compressional wave itself.

Similar experiments were carried out on natural rocks as well. Figure 2 shows the reflection spectrum from the corrugated surface of a Bedford limestone specimen. There are only two distinct minima observed in this case. Similar to the previous case, the higher minimum at 2.3 MHz corresponds to the compressional wave in water propagating at 1460 m/s velocity. The lowest one at 1.5 MHz corresponds to the Stoneley wave propagating at 940 m/s. Since there is no sign of perceivable slow wave propagation in this sample, the lowest minimum is missing and the Stoneley wave can be regarded as a true interface mode, as in the case of a homogeneous solid immersed in water. Figure 3 shows a similar reflection spectrum from the corrugated surface of a Mt. Helen tuff specimen. Since the shear velocity of this particular rock is higher than the sound velocity in water, the higher maximum at 2.8 MHz corresponds to a leaky Rayleigh mode propagating at 1780 m/s velocity. The lower minimum at 1.95 MHz corresponds to the Stoneley wave propagating at 1250 m/s velocity. Here again, there is no clear indication of slow wave propagation in the rock specimen, although some ripple is apparent on the lower part of the spectrum, probably caused by incoherent scattering and inevitable uncertainties in the gating process.

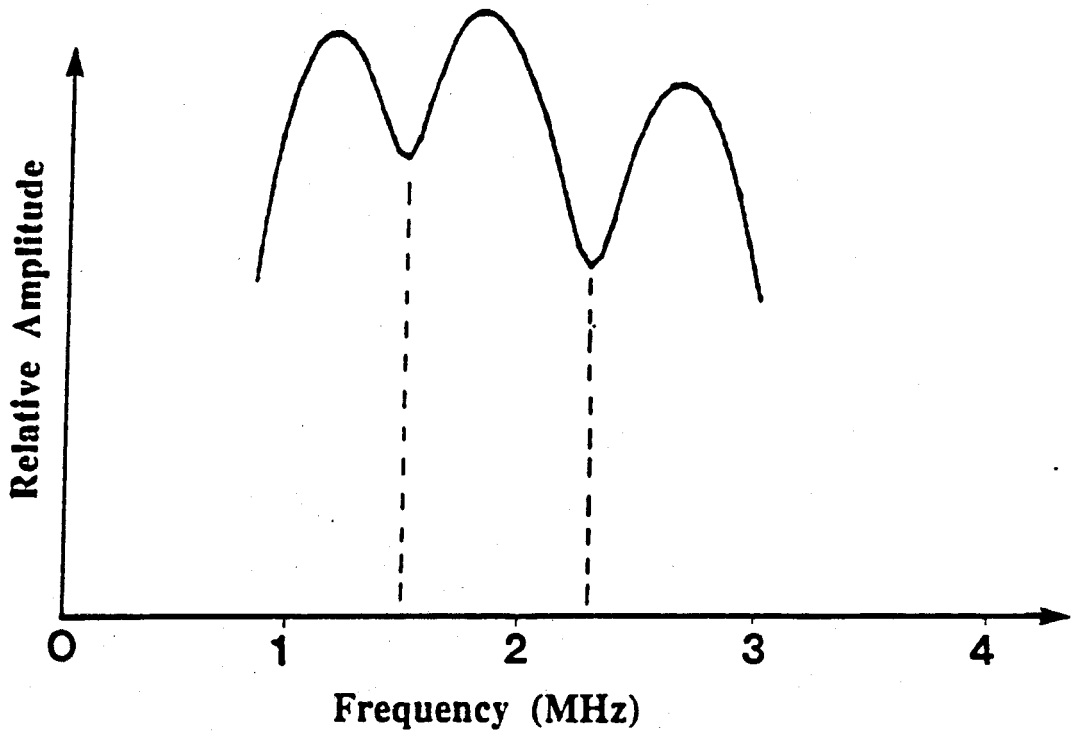

Fig. 2. Deconvolved spectrum of the backscattered signal from a water-saturated porous rock (Bedford Limestone) periodic interface, period = 635 μm, depth = 320 μm.

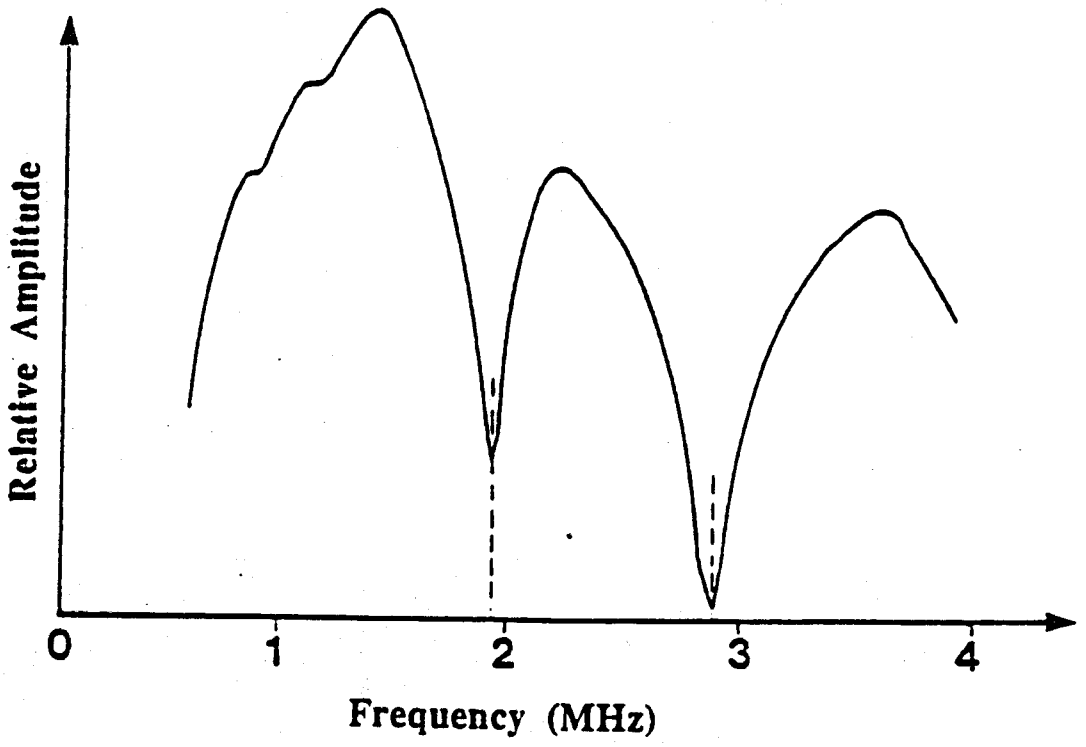

Fig. 3. Deconvolved spectrum of the backscattered signal from a water-saturated porous rock (Mt. Helen tuff) periodic interface, period = 635 μm, depth = 320 μm.

1.2 Direct Excitation Technique

Recently, we have developed a new experimental technique for surface and interface wave generation by direct excitation using conventional contact transducers [5]. This method can be readily used to generate and detect Stoneley waves on a liquid-solid interface, too. The schematic diagram of the suggested interface wave generation technique is shown in Fig. 4. A contact transducer is placed directly over the interface region so that it can generate bulk modes in the upper and lower half-spaces, as well as interface waves along the boundary. In this particular case, we use a shear transducer of vertical polarization, therefore there is a transverse bulk wave in the lower solid medium, but there is no bulk mode in the upper, either air or liquid, medium capable of transmitting compressional waves only.

Figure 5 shows the shear-type bulk and Rayleigh-type surface wave echoes detected from the corner of a 1" long aluminum sample in air. It is important to notice that the bulk signal is much sharper, i.e. it has much more high-frequency components than the surface mode. This difference raises the question of energy partition, i.e. how the total radiated energy is divided between the two principal modes of wave propagation. That part of the transducer which is directly over the interface region within approximately one wavelength generates mostly interface modes, while the other part which is farther away from the interface generates mostly bulk modes. According to this very simple model, the total energy will be partitioned between the interface and bulk modes proportionally to the wavelength-to-radius ratio. Since the

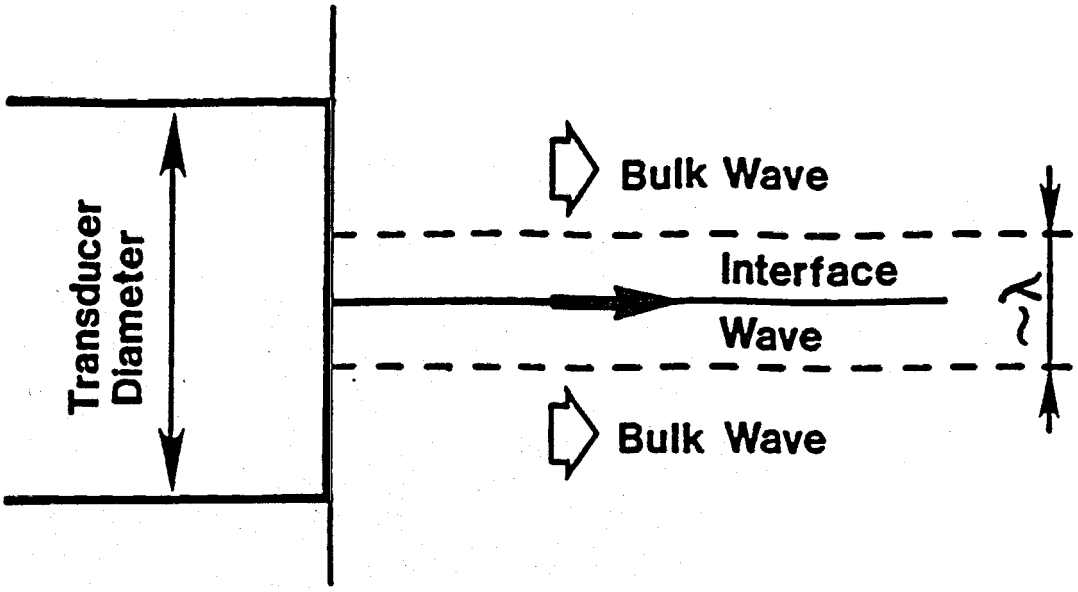

Fig. 4. Schematic diagram of interface wave generation by direct excitation.

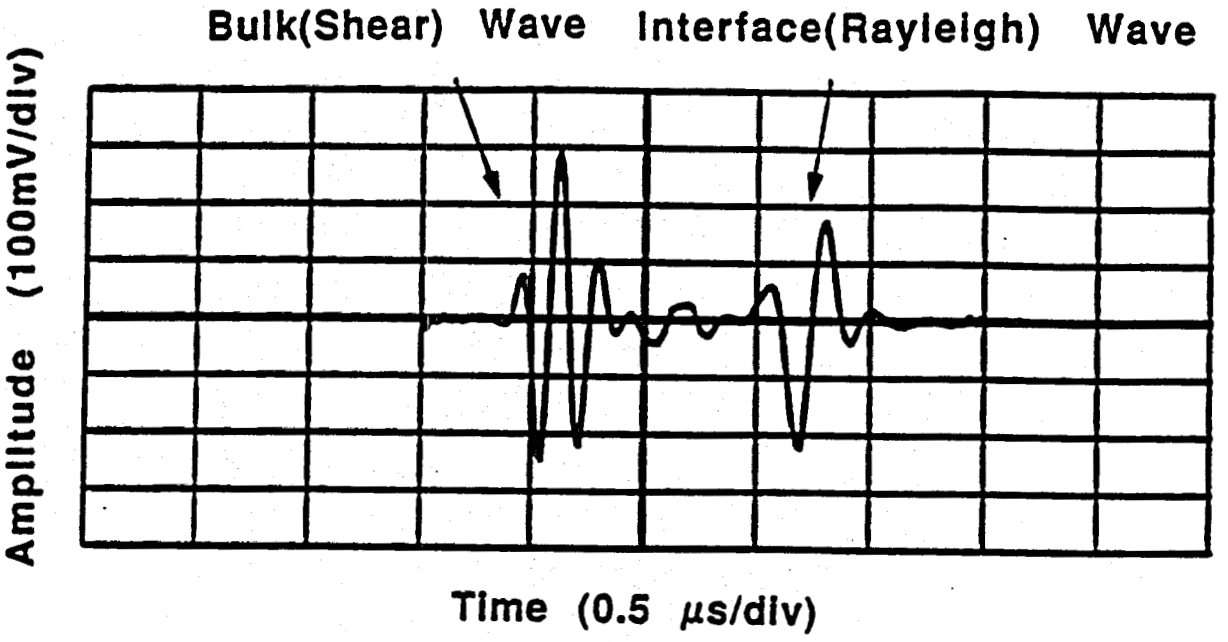

Fig. 5. Bulk and interface wave reflections from the corner of a 1" long aluminum specimen.

wavelength is inversely proportional to frequency, the low-frequency components contribute to the interface mode only while the high-frequency components go to the bulk mode. This conclusion is confirmed by Fig. 6 showing the complemental frequency spectra of the two principal pulses of Fig. 5. Since, as we are going to see later, the high-frequency components are much more attenuated in porous materials, such as rocks, than in aluminum, the interface mode becomes the dominating one in most cases.

Our main interest lies in the generation of the Stoneley-type interface mode at a liquid-solid boundary. Figure 7 shows the phase velocity of this mode as a function of the longitudinal velocity in the solid for a given Poisson's ratio of 0.3. Two curves for n = 1 and 3 density ratios between the solid and the liquid are shown (these density ratios can be regarded as approximate minimum and maximum values for natural rocks). Also plotted is the Rayleigh wave velocity on the free surface of the solid and the compressional wave velocity in the fluid, assumed to be water. The Stoneley wave velocity is always lower than both the Rayleigh velocity for the solid and the sound velocity in the fluid. As an example, the Rayleigh and Stoneley velocities are shown by solid and open squares, respectively, for plexiglas. In this particular case, the surface wave velocity drops from 1270 m/s to 1042 m/s as the plexiglas is immersed in water. These values are typical for natural rocks as well, while most solids of higher density and longitudinal velocity have Stoneley wave velocities just below the sound velocity in water.

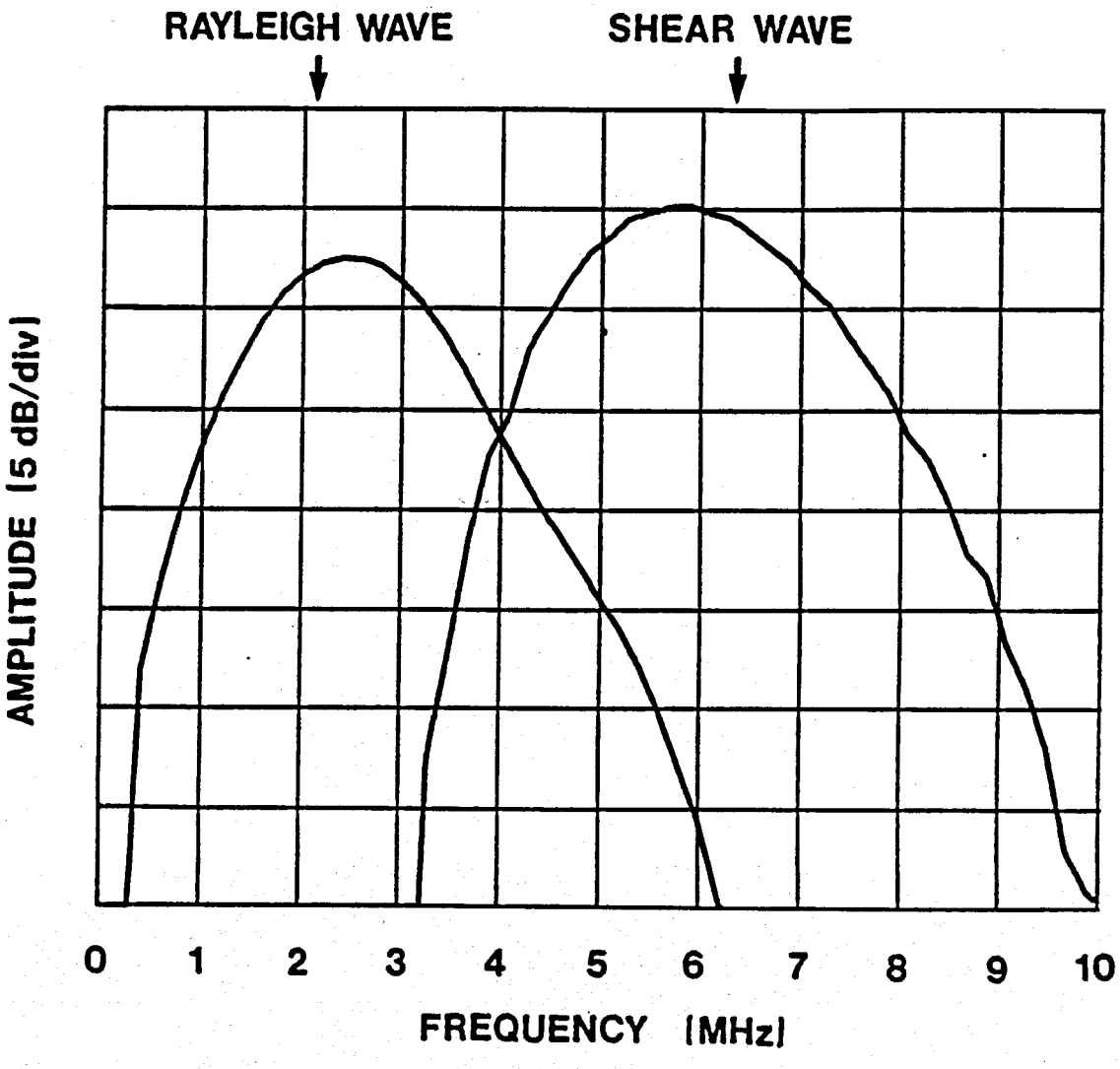

Fig. 6. Frequency spectra of the Rayleigh and shear pulses shown in Fig. 5.

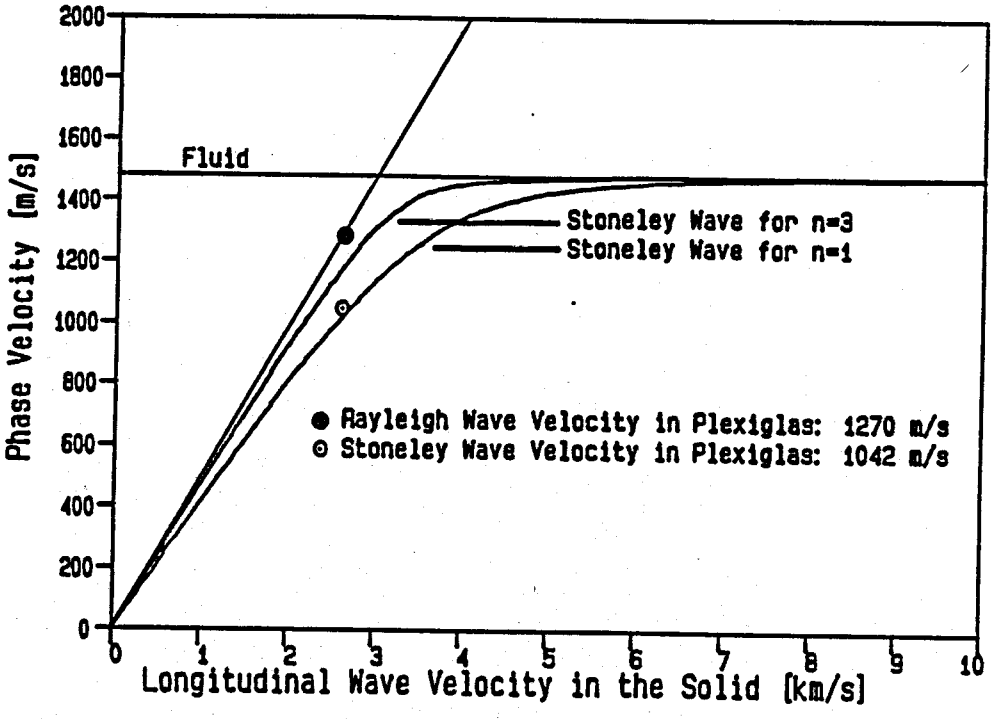

Fig. 7. Stoneley wave velocity as a function of the longitudinal velocity in the solid for two different density ratios.

Figure 8 shows the continuous transformation of the Rayleigh-type surface mode into a Stoneley-type interface mode on the surface of a 42 mm long plexiglas sample as it is gradually immersed in water. The shear pulse is very weak because of the substantial attenuation in plexiglas at high frequencies, and it is not affected by the immersion. The Stoneley wave is slightly more attenuated than the Rayleigh mode, and it comes approximately 14 μs later. The Stoneley velocity obtained from this experiment is 1046 m/s which agrees very well with the calculated value of 1042 m/s.

The practical advantages of the suggested direct excitation technique over the formerly used corrugated surface technique are quite obvious. The crucial question is whether or not it can be used on natural rocks. As an example, Fig. 9 shows the Rayleigh and Stoneley wave pulses detected along the surface of a 28 mm long Mt. Helen tuff specimen. Because of the very high attenuation, single transmission was used with two shear transducers instead of the single-transducer technique with corner reflection. The Rayleigh and Stoneley velocities were found to be 1540 m/s and 1300 m/s, repsectively. The Stoneley wave velocity can be determined from the corrugated surface measurements as 1250 m/s, fairly good agreement with the direct excitation technique.

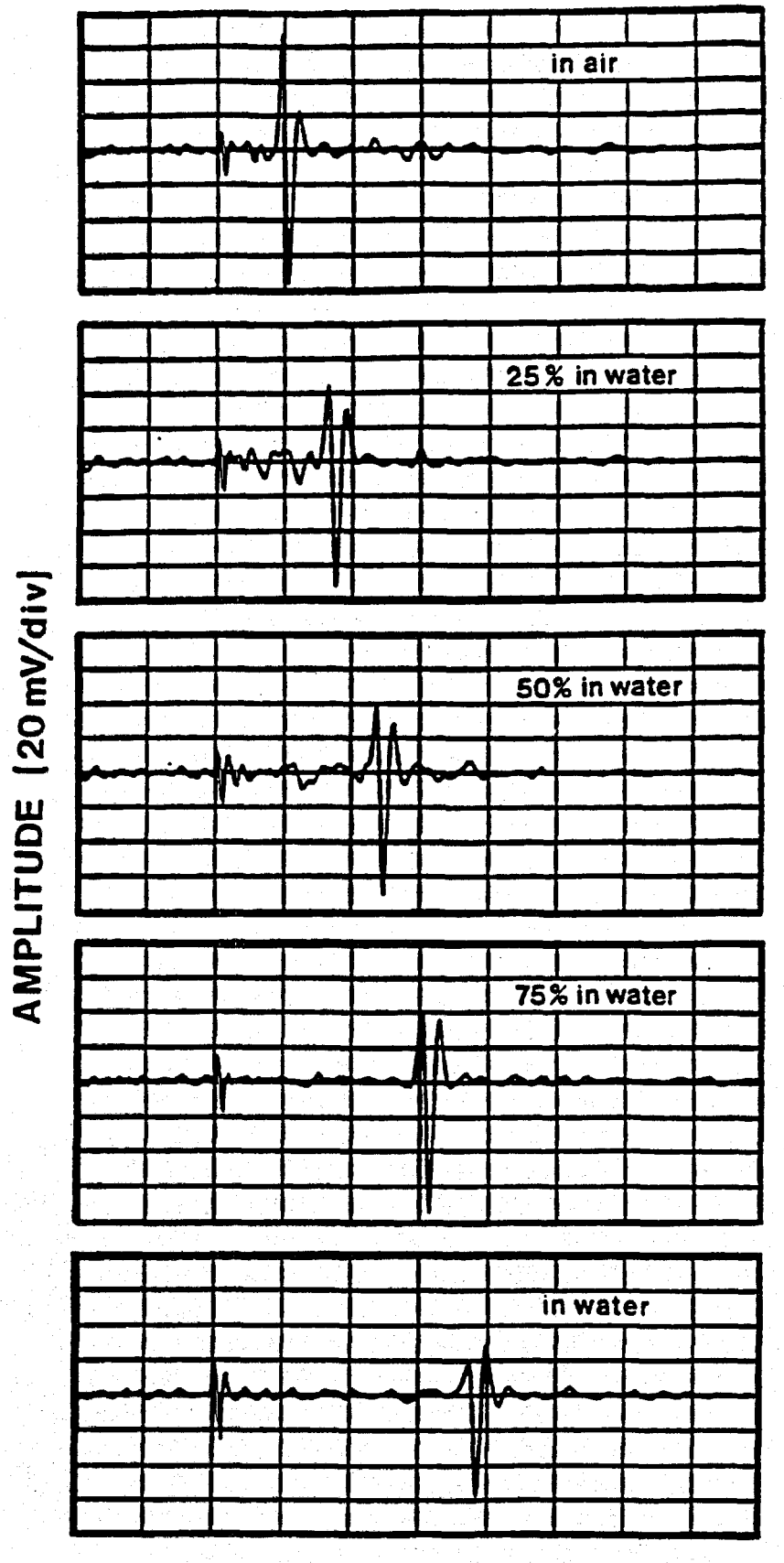

Fig. 8. Continuous transformation of the Rayleigh mode into Stoneley mode on the surface of a 42 mm long plexiglas sample as it is gradually immersed in water.

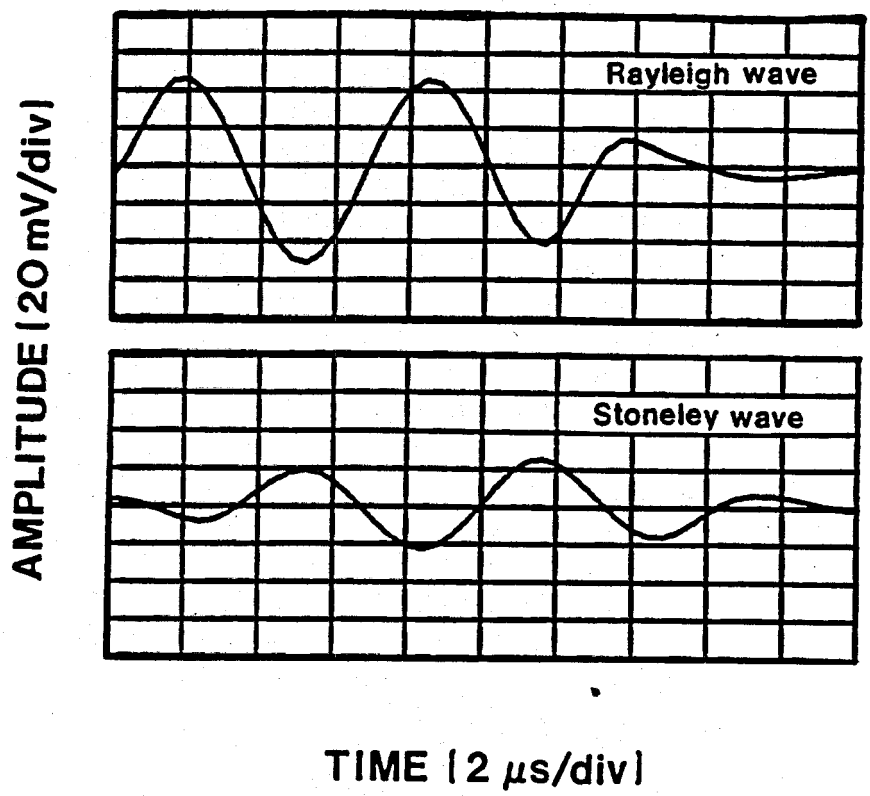

Fig. 9. Rayleigh and Stoneley wave pulses along a 28 mm long sample of Mt. Helen tuff.

2 REFLECTION AND TRANSMISSION OF ELASTIC WAVES AT BOUNDARIES BETWEEN FLUID AND FLUID-SATURATED POROUS SOLIDS

2.1 Introduction

Biot [6] first established a simple and effective two-phase theory for the acoustics of porous media in the mid-1950's. One fundamental feature of this theory is the prediction that there always exists both a fast and a slow compressional mode, as well as a shear mode, in a fluid-saturated porous solid. However, direct experimental observation of the slow compressional bulk wave at MHz frequency was not achieved until 1980 by Plona [7]. Plona's technique is based on the mode conversion of an incident compressional wave (in the fluid) into fast, slow, and shear wave in the fluid-saturated porous media. In order to estimate the relative amplitudes of the various waves generated at the interface, one needs to address the problem of the elastic wave reflection and transmission at the boundary between the two materials. Very few quantitative results on this subject have been published. Most of these were obtained only for certain special cases. Geerstma and Smit [8] solved the problem of reflection and transmission at the interface of two porous media in the case of normal incidence. Deresiewicz and Rice [9] derived the solution for the reflection of elastic waves from a free surface of a fluid-saturated porous solid. Stoll, et. al [10] studied the reflection and refraction of an inhomogeneous plane acoustic wave incident from water to a half-space composed of porous sediment. However, Stoll did not consider the effect of the pore boundary condition and did not

identify the refracted fast and slow compressional waves and the shear wave.

In the main frame of our work [11], we develop a numerical solution approach to deal with the problem of reflection and transmission of elastic waves at a fluid/porous solid interface for the case of general boundary conditions and oblique incidence. Particular attention is given to the effect of the pore surface boundary condition of the reflection and transmission coefficients. The energy reflection and transmission coefficients as a function of incident angle are obtained. The key point here is to derive the expressions of the energy equation and Poynting energy flux vector for various elastic modes in a fluid-saturated porous solid. Furthermore, the transmission of elastic wave through a fluid-saturated porous solid plate immersed in fluid is calculated. Mesurement of sound transmission through porous plate was carried out by using experimental techniques suggested by Plona [7]. Good correlation between measured and calculated values of the angular behavior of the transmission coefficients for fast, shear, and slow waves was obtained after adjusting the theory for experimentally obtained attenuation using artificial rocks.

2.2 Theory

We consider the following configuration of the problem: one half-space filled with fluid and another half-space occupied by the fluid-saturated porous solid, separated by an interface. The porous medium is a macroscopically homogeneous, isotropic, and fluid-saturated porous solid, so potential functions for fast and slow compressional and shear waves can be used to compute the reflection and transmission coefficients. Boundary conditions at the interface are adopted from Feng and Johnson [1].

2.3 Numerical Results

Two general cases of mode conversion have been investigated: (1) the initial wave is incident from the fluid to the interface and generates three transmitted bulk waves in the fluid-saturated porous solid, and (2) the initial wave is incident from the fluid-saturated porous solid to the interface and generates three reflected bulk waves in the same medium. Furthermore, the transmission of sound energy in the form of fast, slow compressional, and shear waves through a fluid-saturated porous solid plate immersed in fluid is calculated.

The numerical results for energy reflection and transmission coefficients for a compressional wave incident from a fluid on a fluid/porous solid interface for the open pore and sealed pore boundary conditions are shown in Figs. 10-12. The porous material is a water-saturated fused glass bead solid whose physical parameters are listed in Fig. 10. The corresponding phase velocities for the fast and slow compressional waves and the shear wave are $V_+ = 2657$ m/s, $V_- = 935$ m/s, and $V_{sh} = 1281$ m/s; the phase velocity of water is $V_f = 1500$ m/s. Because $V_+ > V_f$ there is a critical angle of about 34.4°. Generally, the reflection and transmission coefficients change very sharply in the vicinity of the critical angle. At this critical angle, the energy reflection coefficients are maximum and transmission coefficients are minimum. Beyond this critical angle, the transmitted fast compressional wave in the water-saturated porous fused glass bead solid is evanescent in the z-direction. It is seen from these figures that the energy

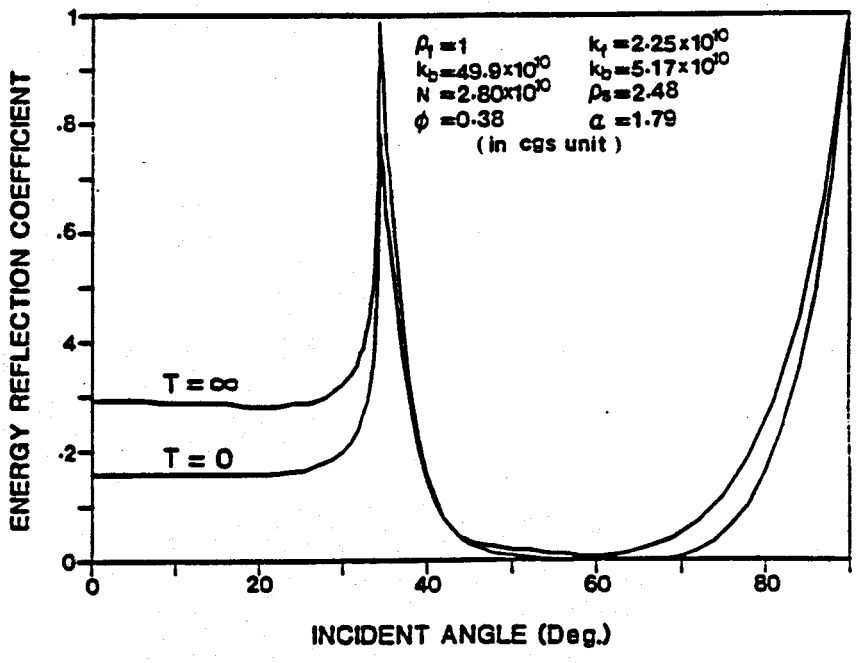

Fig. 10. Energy reflection coefficients of a compressional wave incident from water on an interface between water and water-saturated porous fused glass bead solid with open pore (T = 0) and sealed pore (T = ∞) boundary condition.

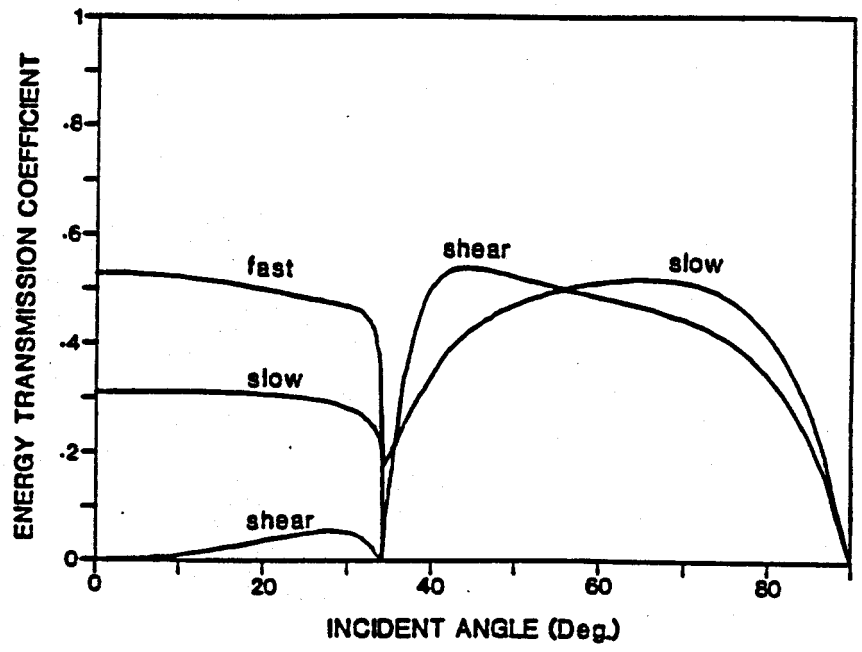

Fig. 11. Energy transmission coefficients of a compressional wave incident from water on an interface between water and water-saturated porous fused glass bead solid. Open pore boundary conditions were assumed.

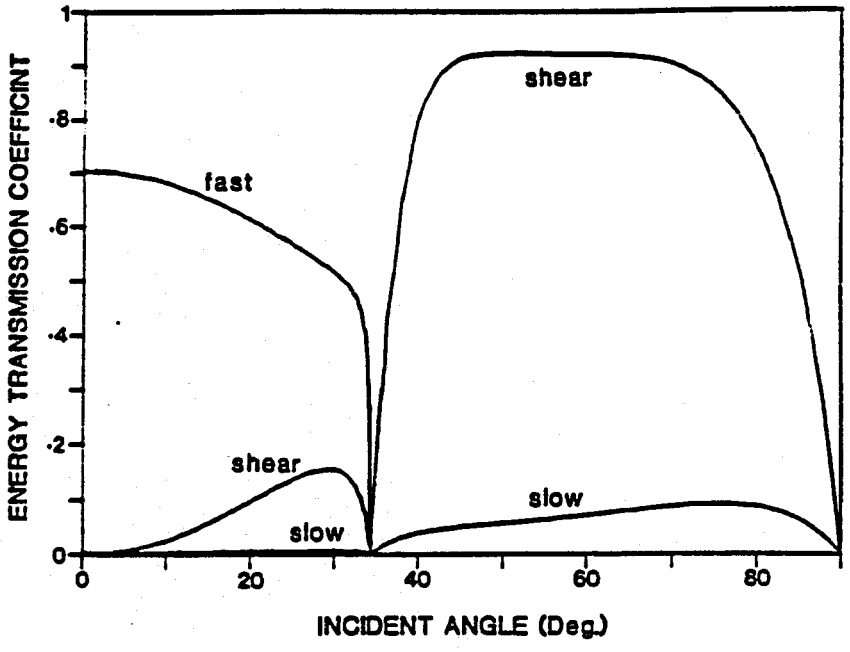

Fig. 12. Energy transmission coefficients of a compressional wave incident from water on an interface between water and water-saturated porous fused glass bead solid. Sealed pore ($T = \infty$) boundary conditions were assumed.

transmission coefficient of the slow compressional wave for the sealed pore case is much less than that for the open pore case, but the energy transmission coefficients of the fast compressional wave and the shear wave in the sealed pore case are greater than those for the open pore case due to the conservation of total energy.

When the incident wave (which may be fast or slow compressional or shear) originates in a fluid-saturated porous solid to the fluid, three reflected bulk waves in the porous solid and one transmitted compressional wave in the fluid will be generated. For these cases, we have also calculated the angular dependence of energy reflection and transmission coefficients. For more details, we reference our paper [11].

Using the above-mentioned numerical solutions for energy reflection and transmission coefficients of elast waves from a fluid/porous solid interface, we have also calculated the transmission of sound through a fluid/fluid-saturated porous solid/fluid system (Fig. 13).

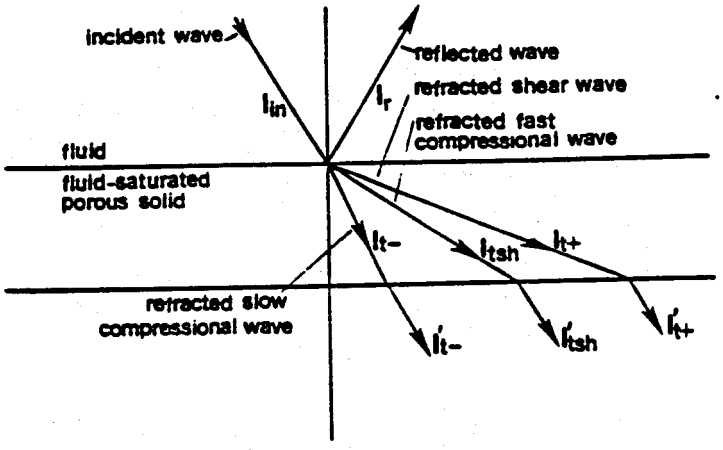

Fig. 13. Mode conversion and refraction at liquid-porous/ solid-liquid interface (reflected waves are not shown).

2.4 Experimental Results

In order to compare our theoretical predictions to experimental data, we carried out measurement of reflection and transmission coefficients. Figures 14 and 15 show the theoretical prediction and experimental results of energy reflection coefficients for open pore and sealed pore boundary conditions. The porous material selected for experimental investigation is the artificially fused glass bead (PG15). For sealed pore samples, a thin coat of paint on the interface eliminates fluid flow between the saturated porous medium and the surrounding fluid; for open pore samples, not having a coat of paint allows free fluid motion. These experiments were performed in a water tank at 0.5 MHz frequency using a two-transducer immersion technique. It has been shown that the experimental results are in good agreement with the theoretical curves.

Figures 16-18 show the theoretical predictions and experimental results of transmission coefficients through a water-saturated porous solid plate using the technique described by Plona [7]. An ultrasonic immersion technique was used to generate bulk modes in the water-saturated porous solid plate. Due to mode conversion at the interfaces and because of their different velocities, the fast, slow, and shear waves are separated in time. The transmitted amplitudes of the corresponding waves at various angles were measured and normalized with the incident amplitude. In order to compare theoretical predictions to experimental data, the theoretical curves were corrected for attenuation. The attenuation coefficients (assuming center frequency for each case) are for fast wave, $\alpha = 0.35$ dB/mm MHz, for shear wave, $\alpha = 1.34$ dB/mm MHz, and

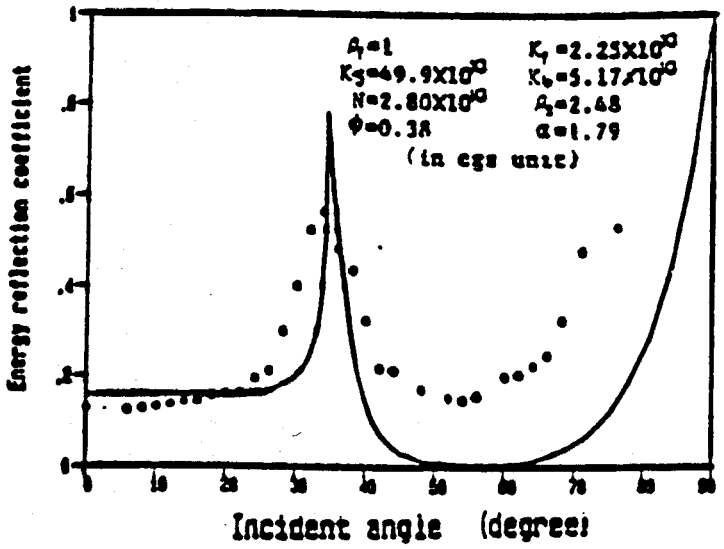

Fig. 14. Energy reflection coefficient for open pore (T = 0) boundary condition.

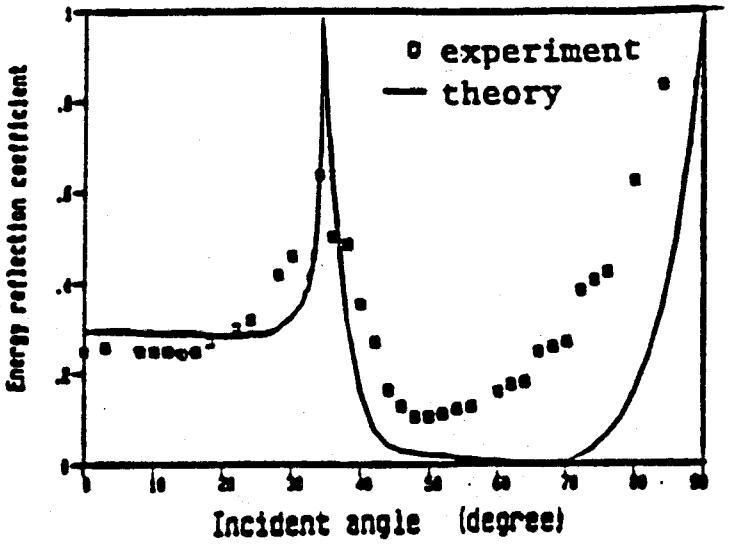

Fig. 15. Energy reflection coefficient for sealed pore ($T = \infty$) boundary condition.

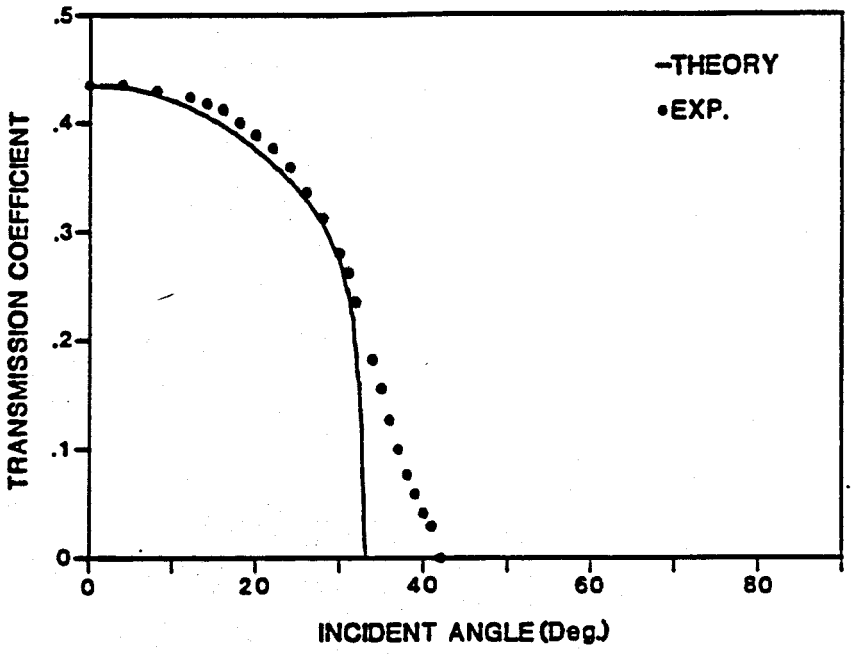

Fig. 16. Comparison of theoretical (solid line) and experimental (dotted line) transmission coefficient vs. angle of incidence for fast wave through a water-saturated porous fused glass bead plate immersed in water.

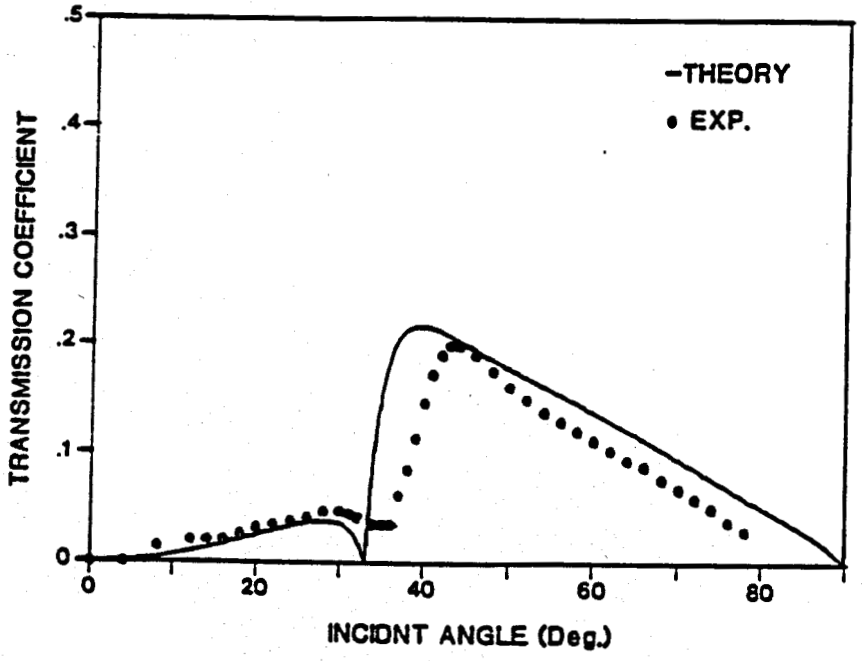

Fig. 17. Comparison of theoretical (solid line) and experimental (dotted line) transmission coefficient vs. angle of incidence for mode converted shear wave through a water-saturated porous fused glass bead plate immersed in water.

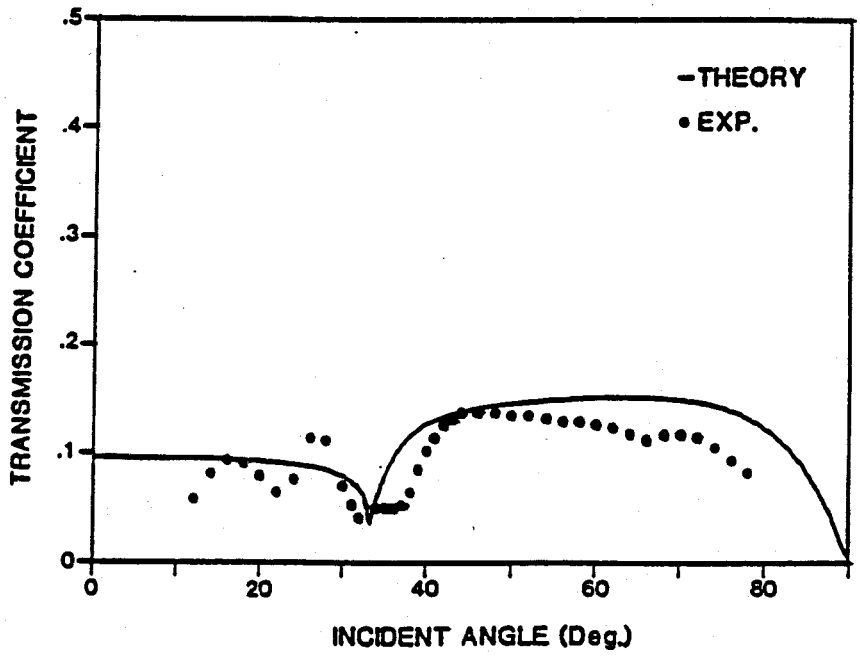

Fig. 18. Comparison of theoretical (solid line) and experimental (dotted line) transmission coefficient vs. angle of incidence for mode converted slow wave through a water-saturated porous fused glass bead plate immersed in water.

for slow wave, α = 1.8 dB/mm MHz. We found good qualitative agreement between the predicted and measured transmission coefficients.

3 INTERACTION OF ULTRASONIC WAVES WITH THIN FLUID-SATURATED POROUS PLATES: THEORY AND EXPERIMENTS WITH LAMB WAVE TECHNIQUE

3.1 Introduction

Experimental verification of Biot's theory [6] at ultrasonic frequencies was achieved in 1980 when Plona [7] observed all three bulk waves by using mode conversion techniques on fluid-saturated porous slabs immersed in water. The measurement of the slow compressional wave provides an ultrasonic approach to estimate rock permeability in situ. Although the mode conversion technique has been used successfully in detecting slow waves in various synthetic porous media, it appears that in the majority of porous systems (synthetic or natural porous solids), only one compressional (fast) wave has been observed. The lack of seeing the second compressional wave (or slow wave) in these media, especially in natural rocks, can be attributed to various attenuation mechanisms of the porous structure. For example, the unconsolidation of the porous frame [12] and the deposition of clay particles on the pore walls [13] could prohibit the propagation of the slow wave. In addition to the material properties, in many porous systems the lack of seeing slow waves is due to excessive attenuation of ultrasound caused by scattering of pores. A feasible way to reduce the attenuation of ultrasound is to reduce the thickness of the porous samples to be measured. However, for a thin porous slab it is inadequate to use the mode conversion technique to detect the slow wave because signals expected from the slab are usually overlapped by multiple reflection signals due to faster waves and, therefore, are undetectable.

To overcome this problem efforts are made in the present work to explore a novel experimental strategy for measuring the slow wave in thin fluid-saturated porous plates by using Lamb modes. Since analysis by Rayleigh [14] and Lamb [15], the vibration modes for an elastic homogeneous solid thin plate are well understood. These so-called "Lamb modes" result from a pure compressional wave and pure shear wave. Similarly, excitation of "leaky Lamb modes" in elastic plates immersed in a fluid, caused by incident acoustic waves, has been extensively described theoretically and experimentally [16]. Results are generally presented as dispersion curves which relate the phase velocity of the mode to the product of frequency and plate thickness.

The purpose of this work is to extend this formalism to the particular case of fluid-filled porous thin plates. General solutions for a thin fluid-saturated porous plate are derived to obtain dispersion curves of Lamb modes and to calculate reflection and transmission behavior of ultrasound through the thin porous plate. Based on the theoretical predictions, we propose a new method to detect slow waves in the frequency domain by measuring the Lamb wave spectrum. Experimental studies proving theoretical predictions are performed on synthetic and natural porous plates.

3.2 Theoretical Analysis

3.2.1 Field Solution

The theoretical treatment of Lamb wave propagation in a fluid-saturated porous plate takes into account the existence of the slow compressional wave in addition to the fast compressional wave and the shear wave. To obtain a field solution we assume that the porous plate complies with Biot's theory [6]. We consider three bulk waves propagating in the plate. Using the geometry and the coordinate system given in Fig. 19, the potential functions for fast, slow, and shear waves can be written as

$$\Phi_+ = (A_1 \cosh \gamma_+ Z + A_2 \sinh \gamma_+ Z) \exp[i(kx - \omega t)], \quad (1)$$

$$\Phi_- = (A_3 \cosh \gamma_- Z + A_4 \sinh \gamma_- Z) \exp[i(kx - \omega t)], \quad (2)$$

and

$$\Psi = (A_5 \sinh \gamma_s Z + A_6 \cosh \gamma_s Z) \exp[i(kx - \omega t)], \quad (3)$$

respectively, where γ and k are related to the velocities of the fast, slow, and shear waves (V_+, V_-, and V_s, respectively) through Biot's wave equations. The phase velocity of Lamb modes is defined by

$$C = \omega / R_e(k). \quad (4)$$

Potential functions of the compressional wave in the upper and lower fluid regions surrounding the plate can be expressed as

$$\Phi_1 = (A_i e^{\gamma_f Z} + A_7 e^{\gamma_f Z}) \exp[i(kx - \omega t)] \quad Z > h/2 \quad (5)$$

$$\Phi_2 = A_8 e^{\gamma_f Z} \exp[i(kx - \omega t)] \quad Z < -h/2 \quad (6)$$

where A_i, A_7, and A_8 represent the amplitudes of the potential function for the incident, reflected, and transmitted waves, respectively.

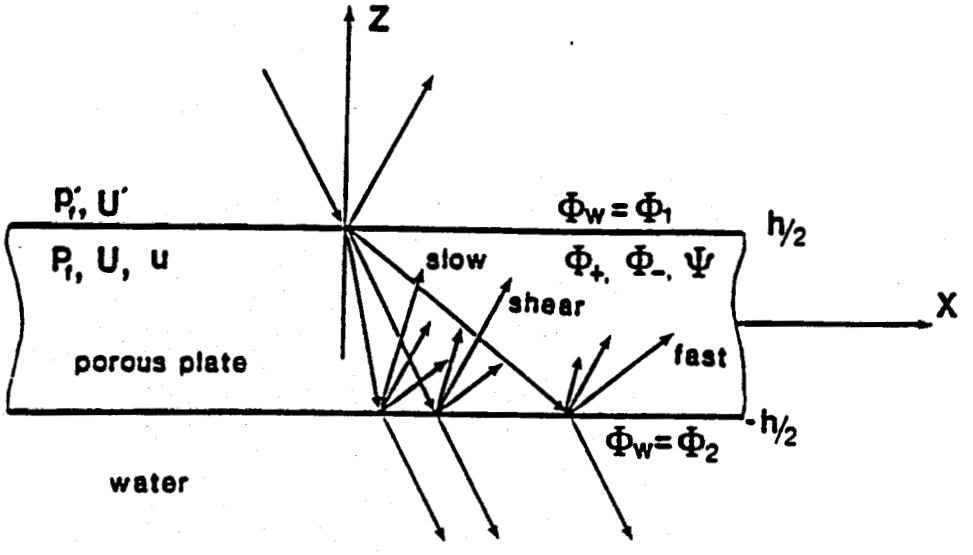

Fig. 19. Scheme of coordinate system for Lamb wave propagation in a fluid-saturated porous plate. Φ_+, Φ_-, and Ψ are potential functions for fast, slow, and shear waves in the porous plate, and Φ_w is the potential of compressional wave in the fluid.

The boundary conditions at a fluid and fluid-saturated porous solid interface were formulated by Feng and Johnson [1] and are not repeated here.

To solve for the eight coefficients, the displacements in both the fluid and the solid skeleton are calculated using the potential functions and then are substituted into the boundary equations at $z = h/2$ and $z = -h/2$, respectively, which results in a matrix form of the characteristic equations

$$\begin{bmatrix} a_{ij} \\ [8x8] \end{bmatrix} \begin{bmatrix} A_1 \\ \vdots \\ A_8 \end{bmatrix} = \begin{bmatrix} b_1 \\ \vdots \\ b_8 \end{bmatrix} A_i \qquad (7)$$

For a given A_i, the reflection and transmission coefficients are determined by

$$R = A_7/A_i \quad \text{and} \quad T = A_8/A_i \qquad (8)$$

which are evaluated as a function of the incident angle (or the phase velocity of Lamb wave) and fh, the product of frequency and the thickness of the plate.

The dispersion relation of Lamb modes in the fluid-saturated porous plate can be obtained also from Eq. 7 by setting $A_i = 0$.

3.2.2 Slow Wave Influence on Dispersion Curve

In order to compare the Lamb wave dispersion curves for a fluid-saturated porous plate to an equivalent solid plate, a simple example is selected. The dispersion curve for a fluid-saturated porous plate with closed pores in air is shown in Fig. 20. The porous plate is made of sintered bronze beads with material properties described in detail in Ref. 17. The influence of the

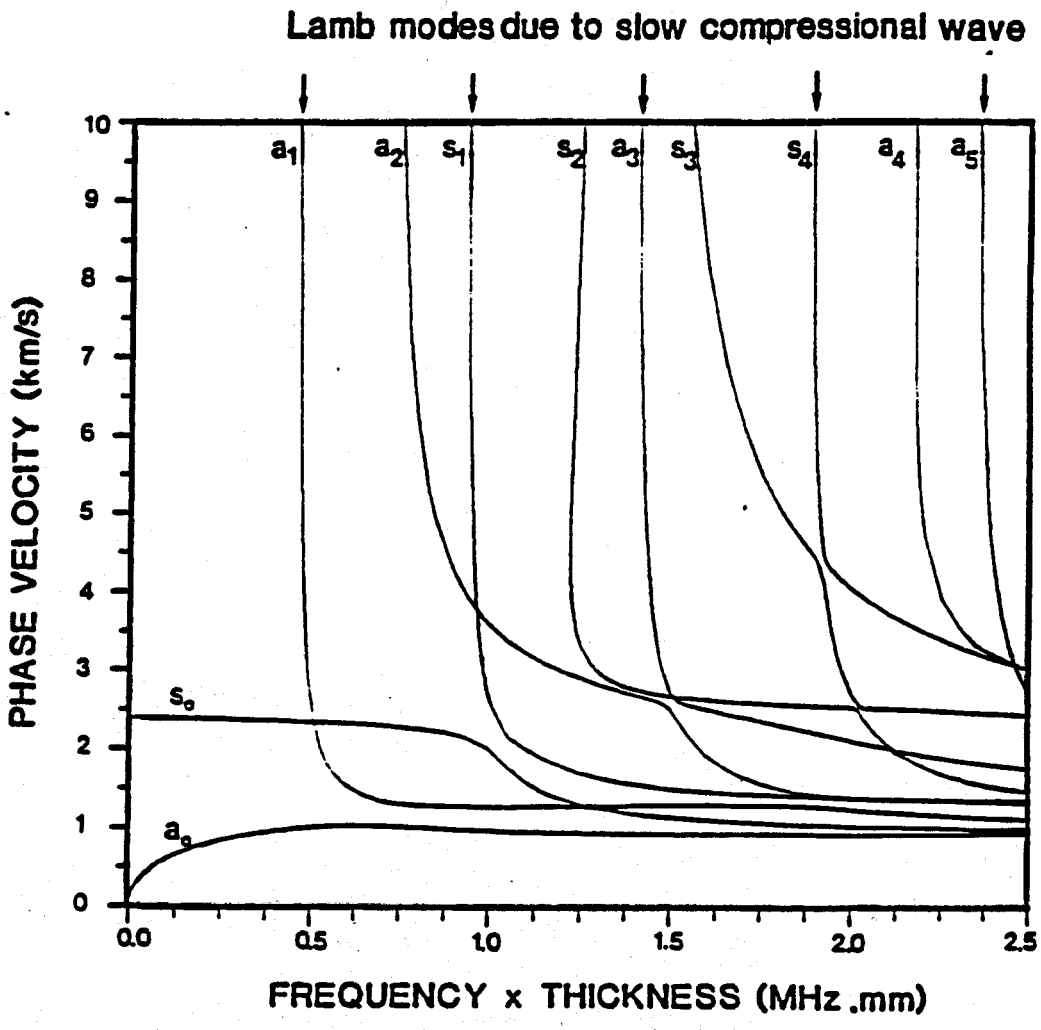

Fig. 20. Dispersion curves of Lamb modes in water-saturated porous plate B05 with sealed pore surface and free boundary.

slow wave on the behavior of the Lamb mode calculations of the dispersion curve can be seen by comparing Fig. 20 to Fig. 21. In Fig. 21, the dispersion curve for a solid plate with the same bulk velocities (as for the porous plate) but without the slow wave is given. In comparing Fig. 20 with Fig. 21, it is obvious that the extra modes A_1, S_1, A_3, S_4, and A_5 in Fig. 20 are due to the presence of the slow compressional wave in the fluid-saturated porous plate. Another feature of Fig. 20 is that it shows that at high frequencies the two lowest modes, S_o and A_o, tend to the velocity of the slow wave instead of the Rayleigh wave velocity as occured in the case of the solid plate.

The most important information provided by Fig. 20 is that the asymptotic values of the Lamb modes at cut-off frequencies can be interpreted by the phase velocities of the three bulk waves and, in particular, the asymptotic values of the above mentioned extra Lamb modes at cut-off are exclusively related to the slow wave velocity.

3.2.3 Experimental Procedure

Fig. 22 shows the scheme of the reflection measurement for Lamb modes in a fluid-saturated porous plate. The plate is immersed in a fluid, being insonified by a 0.5 MHz broadband immersion transducer. The total reflected signal consists of a specular reflected signal and a number of multiple reflection signals (leaky Lamb waves), which are picked up by a 1 MHz broadband immersion transducer. The reference signal of the ultrasonic system is taken from a reflected pulse at an aluminum

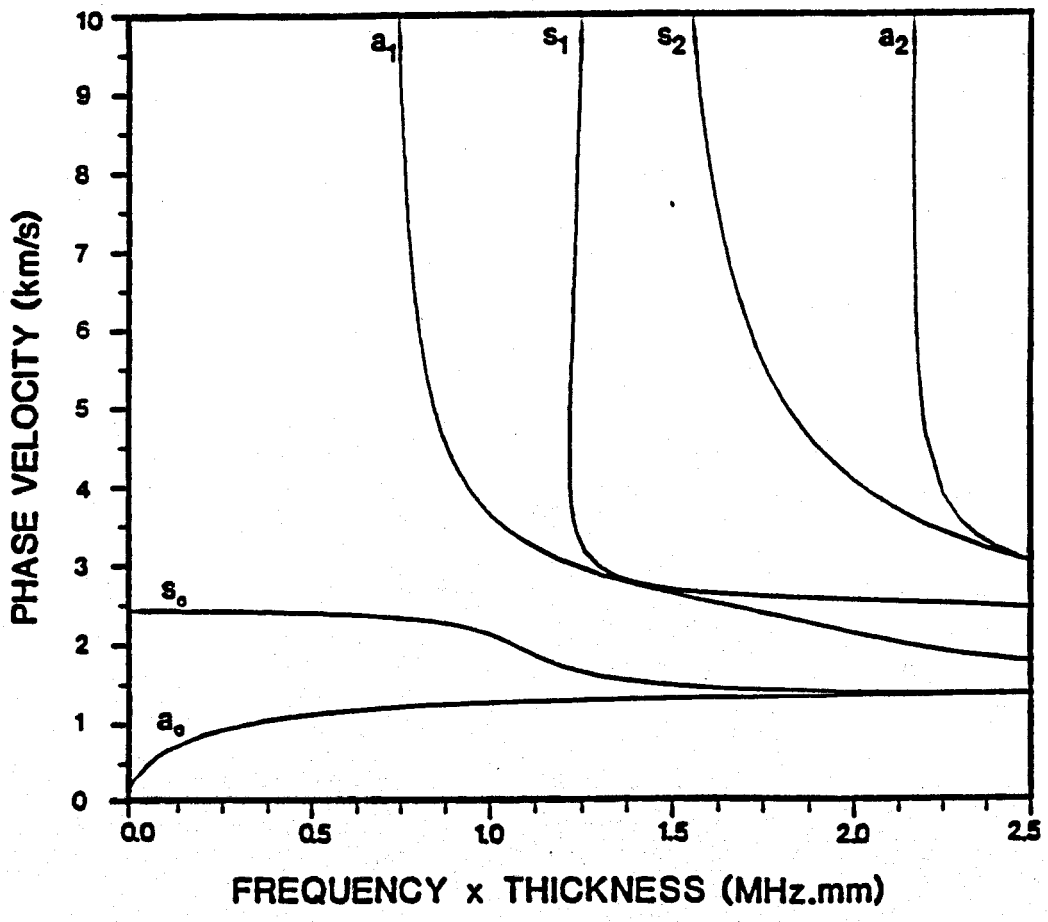

Fig. 21. Dispersion curves of Lamb modes in a free solid plate with ρ_s = 8.6 gcm^{-3}, V_L = 2.586 km/s, and V_S = 1.456 km/s.

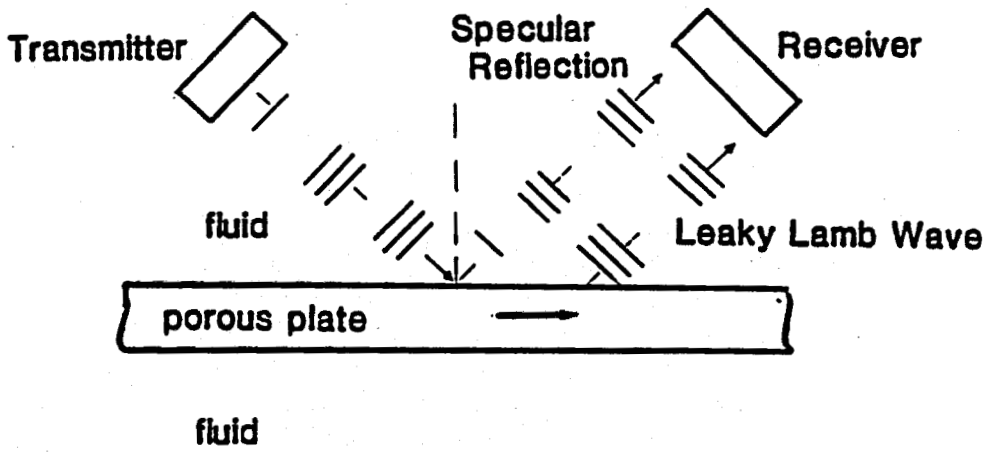

Fig. 22. Scheme of the experimental arrangement.

target and is shown by Fig. 23(a) whose spectrum is presented in Fig. 23(b).

Measurement of Lamb modes is performed by capturing the total reflected signal from a fluid-saturated porous plate at different incident angles. For each given angle, the reflected signal measured in the time domain is converted into the frequency domain by using FFT and then deconvolved from the reference spectrum to eliminate the effect of the system. Figure 24 shows an example of a measured signal and its deconvolved spectrum from a sintered bronze bead plate (sample B05) immersed in water. The deconvolved spectrum shows that there are a number of frequency minima indicated by arrows corresponding to different branches of the Lamb wave spectrum at the given incident angle. The frequency minimum around 0.07 MHz is out of the system bandwidth and caused by noise. The measurement of Lamb modes can also be conducted by capturing the transmitted signal by placing the receiver transducer on the other side of the specimen.

3.2.4 Sample Description

The material properties of the samples studied are described in Table I. Sample B05 is a sintered bronze bead disk with an average grain size of 65 μm. Sample S10 is a sintered stainless-steel bead disk, but the average grain size cannot be statistically measured under a microscope because of irregular grain shapes. The porosity values of the samples are provided by the manufacturer, which are used to calculate tortuosities based on Berryman's relation [18] for spheres. The bulk modulus K_s is determined from

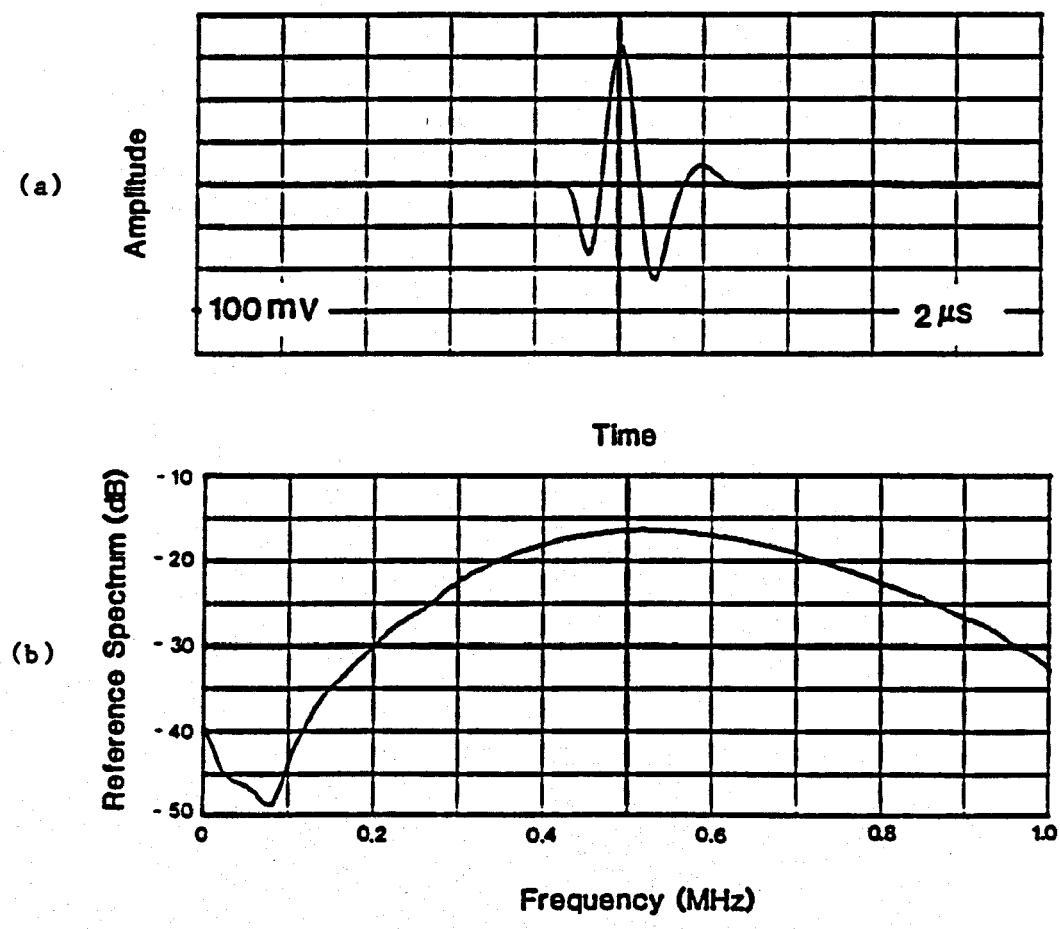

Fig. 23. (a) Reference signal from an aluminum target (incident angle = 14°), (b) Spectrum of (a).

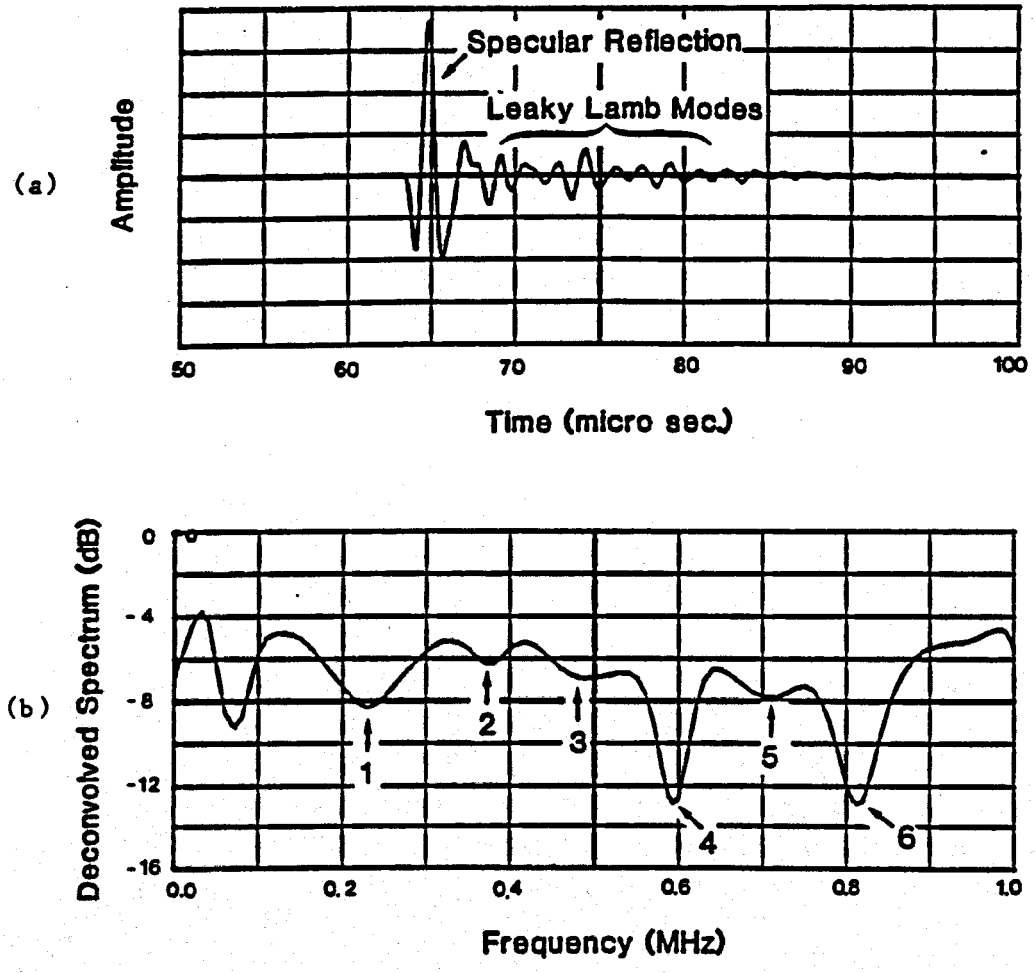

Fig. 24. (a) Measured reflection signals from a water-saturated porous plate (B05) at $\theta = 14°$. (b) The deconvolved spectrum of (a). Arrows indicate the measured frequency minima.

$$K_s = \rho_s(V_{SL}^2 - 4/3V_{SS}^2) \qquad (9)$$

where the solid density ρ_s and velocities of the longitudinal wave V_{SL} and shear wave V_{SS} in the solid material are adopted from the "Handbook of Chemistry and Physics" [19]. V_{FL} and V_{FS}, the velocities of frame longitudinal and frame shear waves in drained porous skeletons are obtained from measurement using contact transducers. The bulk modulus K_b and the shear modulus N are then evaluated from

$$K_b = (1 - \phi)\rho_s(V_{FL}^2 - 4/3V_{FS}^2) \text{ and } N = (1 - \phi)\rho_s V_{FS}^2. \qquad (10)$$

During experiment, the porous plates were saturated with water at room temperature, which has the sound velocity C_F = 1.48 km/s.

By plugging the above parameters into the equations given in [12], the velocities of the fast, slow, and shear waves were obtained as listed in Table I. The data were then used for computing Lamb modes in water-saturated porous plates.

TABLE I. Parameters of Plates B05 and S10 with h = thickness, ϕ = porosity, and α = tortuosity.

	Sintered Bronze Bead Plate (B05)	Sintered Stainless Steel Bead Plate (S10)
h (mm)	2.06	2.06
ρ_s (gcm^{-3})	8.6	7.9
ϕ	30.0	32.0
α	2.17	2.06
V_{FL} (km/s)	2.47	2.886
V_{FS} (km/s)	1.47	1.775
K_s (10^{10} dyn cm^{-2})	143.8	163.6
K_b (10^{10} dyn cm^{-2})	19.5	22.8
N (10^{10} dyn cm^{-2})	13.1	17.4
V_+ (km/s)	2.586	2.971
V_- (km/s)	0.936	0.951
V_s (km/s)	1.456	1.75

3.3 Results and Discussion

3.3.1 Results on Synthetic Porous Plates

To show the correlation between theory and experiment, the results evaluated from spectra of reflection coefficients for porous plates immersed in water are included. Figure 25 shows both theoretical and experimental results for frequency minima of the reflection coefficient measured from sample B05. The data are plotted as a function of the phase velocity of the Lamb modes (vertical axis) and the product of the frequency and sample thickness (horizontal axis). The dotted lines indicate numerical predictions estimated from Eq. 8 by taking only the real part of the Lamb wave velocity. The experimental results were obtained from the measured frequency minima on deconvolved spectra of reflected signals. The measurements have been carried out from incident angle $\theta = 10^{\circ}$ up to 40° with increments of 2.5° for each measurement.

It can be seen from Fig. 25 that the experimental results are in very good agreement with the theory. It should be noted that the horizontal axis of Fig. 25 has an identical unit as the vertical one and that the asymptotic values of measured Lamb modes at cut-off frequencies on the horizontal axis can be interpreted by phase velocities of the three bulk waves. For example, the asymptotic value of the first measurable mode at its cut-off is in coincidence with one-half of the slow wave velocity. From Fig. 24 it can also be seen that those Lamb modes which are relatively insensitive to the change of the Lamb wave velocity are associated

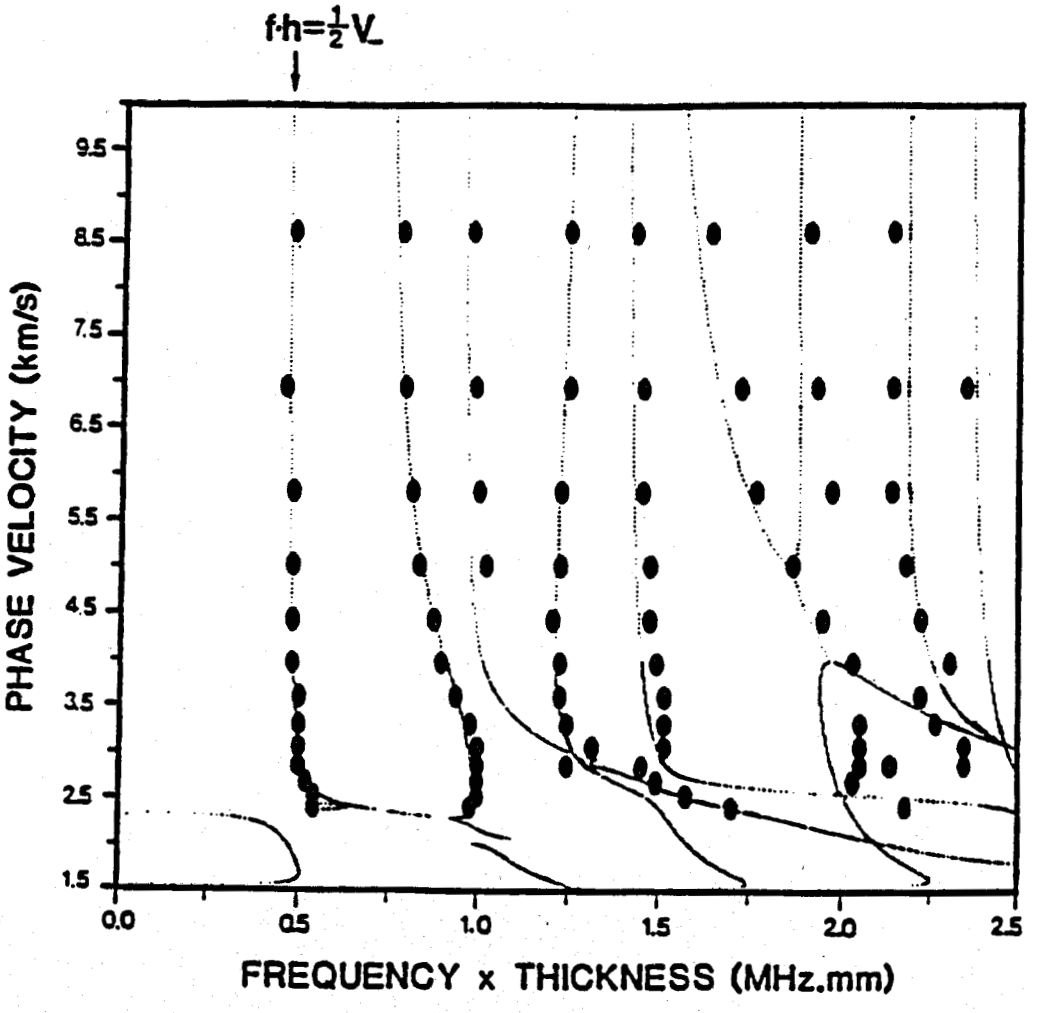

Fig. 25. Frequency minima of reflection coefficient on water-saturated porous plate (B05) immersed in water. ...Theory, • Exp.

with the slow compressional wave.

To further illustrate the correlation between the theory and experiment, a similar result was also obtained from sample S10 and is shown in Fig. 26.

3.3.2 Results on Natural Porous Plates

Following the same procedure performed on the synthetic porous plates, the measurement of the Lamb wave spectrum was also carried out on a number of real rocks. For example, a brown Berea sandstone sample was cut into a thickness of 2 mm and 10 cm in diameter. The tortuosity of three of the samples was estimated by measuring the slow wave velocity in air-filled porous rock. In comparison with any synthetic porous plates, we found the attenuation of ultrasonic signals in the brown Berea sandstone to be much higher. Figure 27 shows the measured reflected signal from the brown Berea sandstone plate at 12.5^{o} using the same system as described before. It can be seen from Fig. 27 that the reflected signal is essentially dominated by the specular reflection. The leaky Lamb modes are highly attenuated and much weaker than in the sintered bronze bead plate (see Fig. 24(a)).

Figure 28 shows the deconvolved spectrum of Fig. 27. Two frequency minima are found at f = 0.23 MHz and f = 0.64 MHz. Because of the high attenuation in the sandstone, indication of the first frequency minimum has a dip less than one-half dB. The location of this frequency minimum gives the estimation of the slow wave velocity at about 0.92 km/sec. The second frequency minimum is due to the fast compressional wave. The absence of

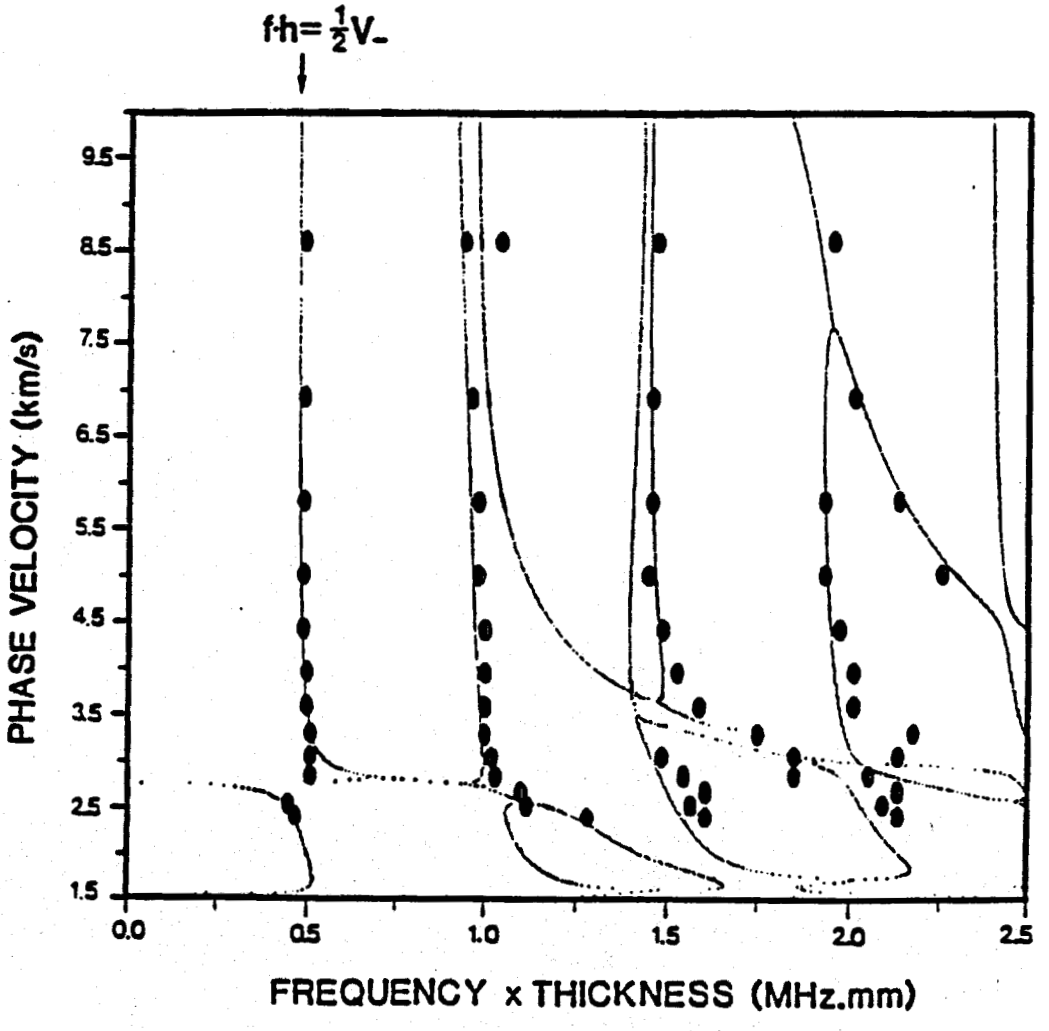

Fig. 26. Frequency minima of reflection coefficient on water-saturated porous plate (S10) immersed in water. ...Theory, • Exp.

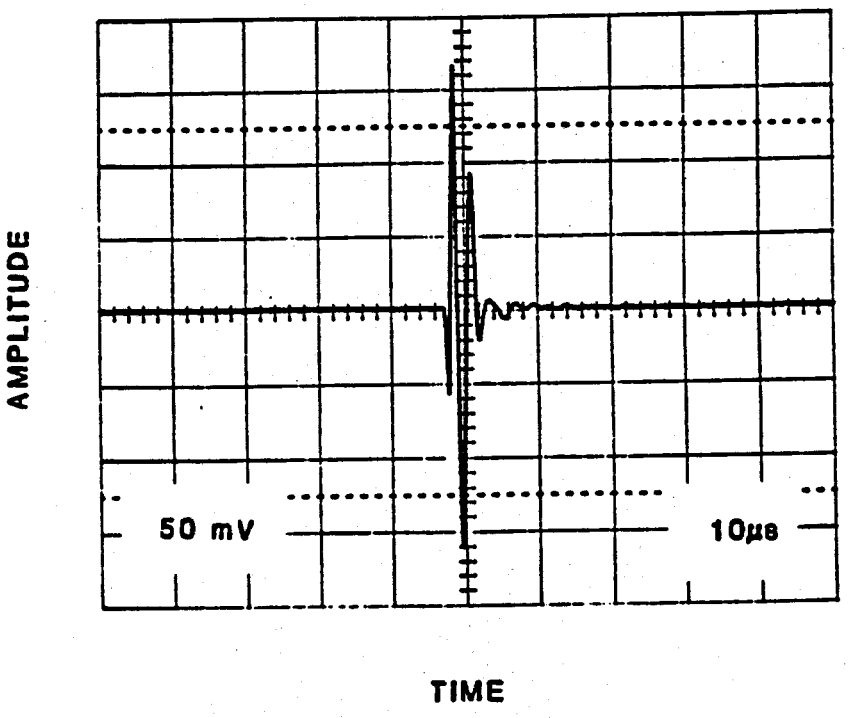

Fig. 27. Reflection signals from a water-saturated brown Berea sandstone plate at $\theta = 12.5°$.

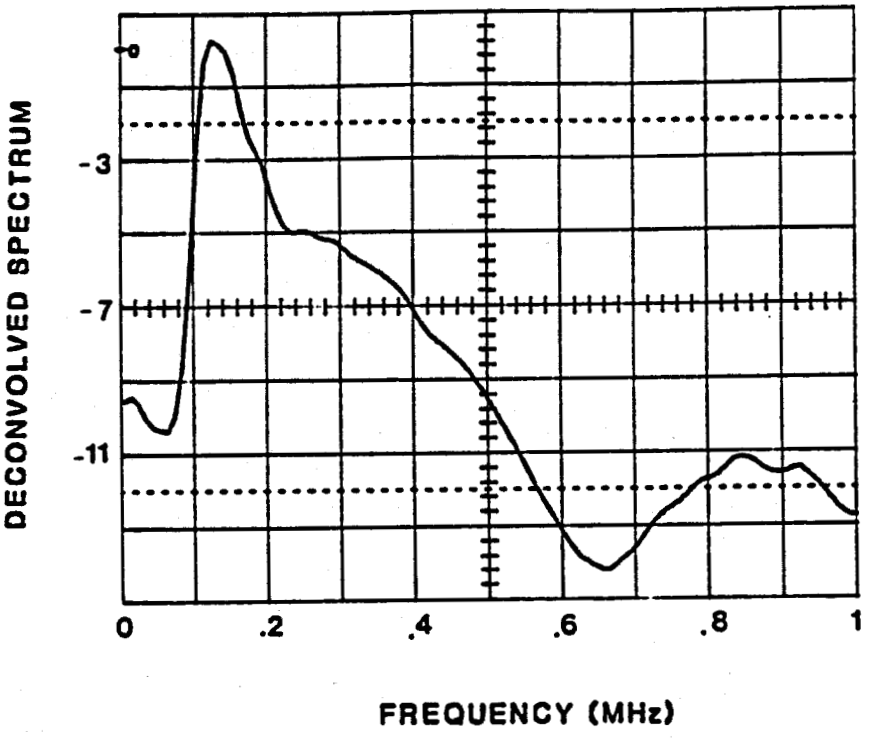

Fig. 28. The deconvolved spectrum of reflection signals measured from brown Berea sandstone at $\theta = 12.5°$.

possible frequency minima between the two indications can be attributed to the low ratio of energy conversion into the shear wave at 12.5°.

3.3.3 Comparison of Bulk and Lamb Wave Techniques

One measure of the increased sensitivity obtained with our newly developed Lamb wave technique is the indication of the presence of slow waves in natural rock (see Fig. 28). No indication of the presence of slow waves in rocks was observed by the bulk wave mode-conversion method. A more quantitative comparison of the two techniques may be obtained by comparing the strength of the slow wave in the porous materal saturated for a certain time with water. In Fig. 29, the amplitude of the slow wave is plotted for time of saturation using both the bulk wave and the Lamb wave technique. At partial saturation, e.g. after a few hours of saturation, the observed slow wave amplitude with the Lamb wave technique is about 10 times as high as observed with the bulk wave technique. Full saturation (measured by the constant value of the slow wave amplitude), attained after 10 hours using Lamb waves, will take over 100 hours using the bulk wave technique.

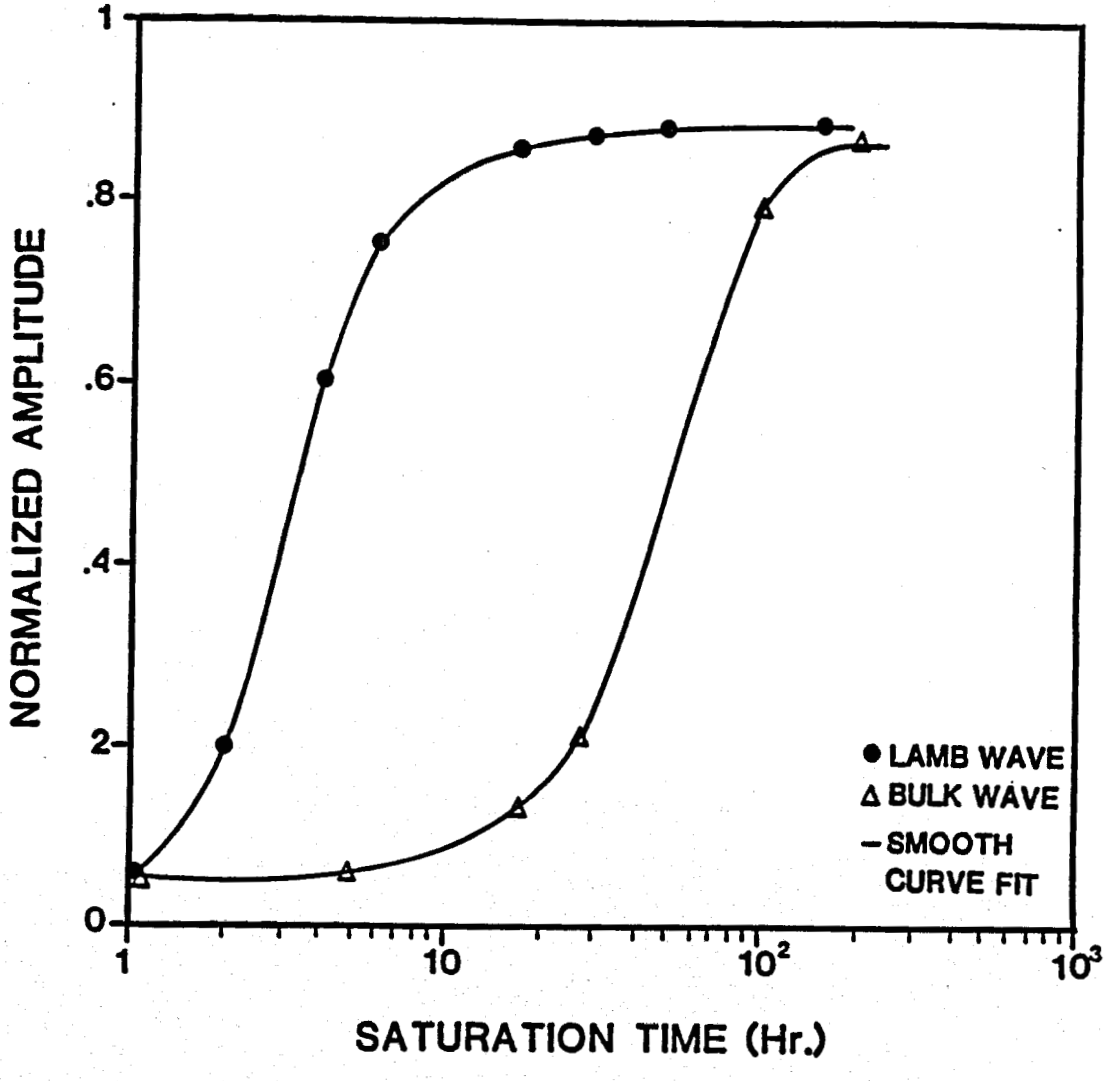

Fig. 29. Measurement of slow compressional wave amplitude vs. saturation time in water-saturated porous glass bead.

4 SLOW WAVE PROPAGATION IN AIR-FILLED POROUS MATERIALS

4.1 Introduction

The main thrust of our former research effort was directed at finding indications of slow wave propagation in natural rocks, which offers a unique acoustical means to evaluate otherwise inaccessible material properties such as tortuosity and permeability. Since 1980, when Plona was able to observe slow wave propagation in artificial rocks made of sintered glass beads [7], the question of why slow waves cannot be detected in real rocks has been one of the major issues in the acoustics of fluid-saturated materials. Recently, it has become more and more evident that whatever was the cause of this lack of perceivable slow wave propagation in natural rocks, it must be an effect not accounted for by the Biot theory. Finally, Klimenatos and McCann showed that the missing detail is associated with inherent internal impurities, such as submicron clay particles, found in all types of natural rocks [13]. These impurities produce three special effects characteristic to real rocks. First, they reduce the porosity of the rock, but this effect is usually negligible. Second, they increase the tortuosity, thereby slightly reducing the expected slow wave velocity. Finally, and most importantly, the clay particles deposited both within the pore throats and on the surfaces of the rock grains greatly increase viscous drag between the fluid and the solid frame, which results in excessive attenuation and complete disappearance of the slow wave.

The question of whether excessive attenuation renders the

detection of slow waves impossible or not arises. Not necessarily! Even a very weak slow wave attenuated by as much as 50-60 dB could be easily detected but for the presence of much stronger background "noise" caused by the direct arrivals and scattered components of the fast compressional and/or shear waves. If we could generate slow wave only and nothing else, it would be much easier to detect it in spite of the substantial attenuation. For example, if there exists a second (shear) critical angle and it is not higher than approximately 60°, then there is no other direct transmission through the fluid-saturated plate at sufficiently high incident angles and even weak slow waves become relatively easy to detect. However, this does not happen in most natural rocks and even if it does, rather strong evanescent waves will be produced in the sample. These vibrations can generate a relatively high scattered background "noise" which renders the weak slow wave signal indistinguishable.

4.2 Theoretical Considerations

An essentially different situation occurs when an air-filled porous sample is insonified by airborne ultrasonic waves. Because of the tremendous acoustical mismatch between the incident compressional wave and the porous solid, all energy is either reflected or transmitted via the slow wave without generating appreciable fast compressional or shear transmitted waves. This crucial effect is well demonstrated by Figs. 30(a) and 30(b) showing the different energy transmission coefficients through a water- and air-saturated porous plate as a function of incident angle. It is quite obvious that in contrast to the water-saturated case, the slow wave is the only vehicle capable of transmitting airborne ultrasound through an air-filled porous specimen.

In spite of the excellent coupling between the incident compressional wave and the transmitted slow wave and the obvious advantage of saturating the specimen with low-viscosity air rather than high-viscosity water, slow wave propagation in air-filled porous samples has never been extensively studied. This is probably due to unusual technical difficulties associated with the generation and detection of airborne ultrasound and to the fact that slow waves are not expected to propagate in air-saturated porous samples as easily as in water-saturated ones [12]. Since the kinematic viscosity of air is so large and the velocity of sound in air is so small, there is but a very narrow frequency window where the attenuation coefficient is sufficiently low to observe a dispersion-free slow wave. This "window" is set by the conditions that the viscous skin depth σ be less than the pore size

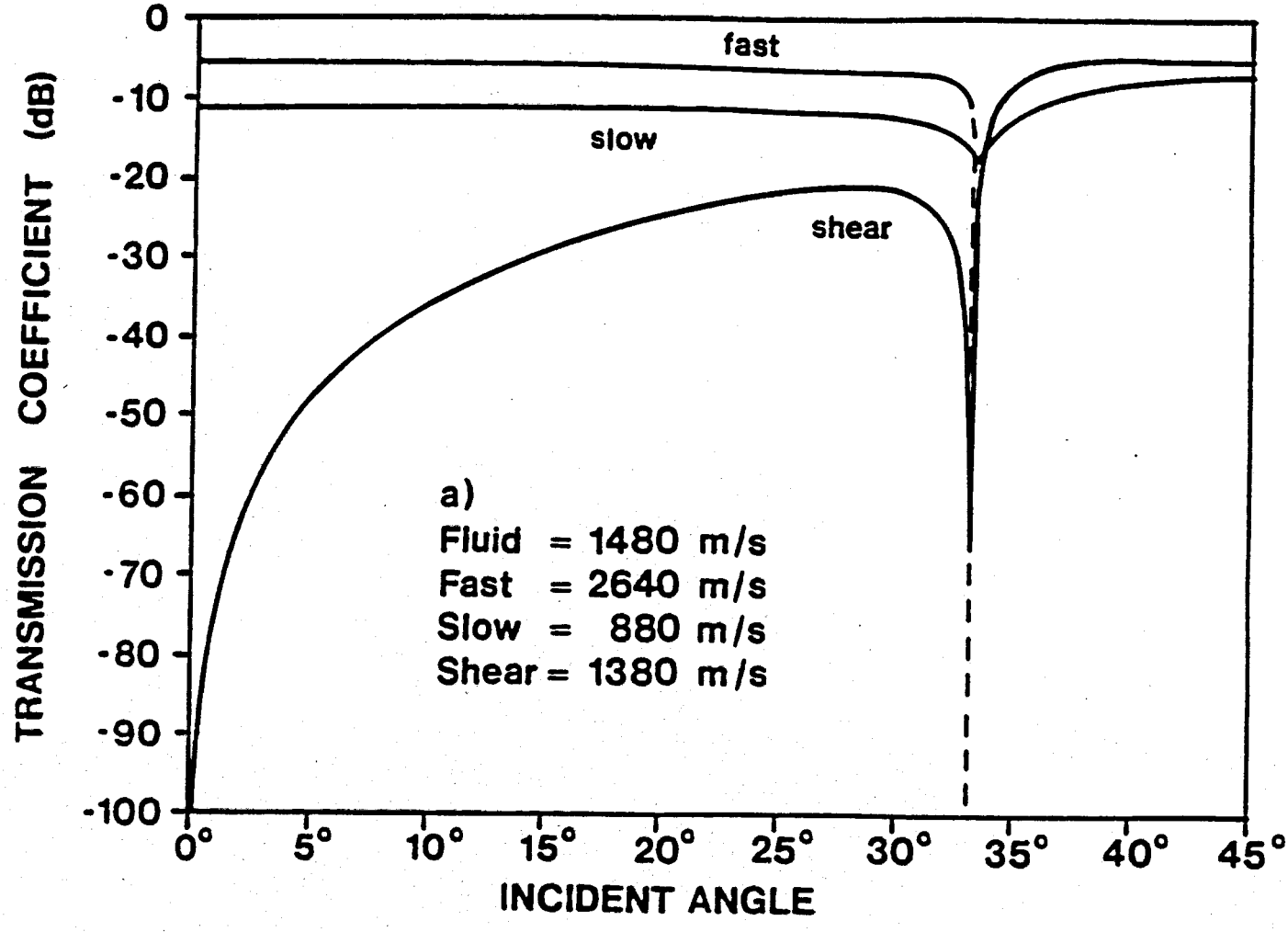

Fig. 30(a). Slow, fast, and shear wave transmission coefficients through water-saturated glass bead specimens.

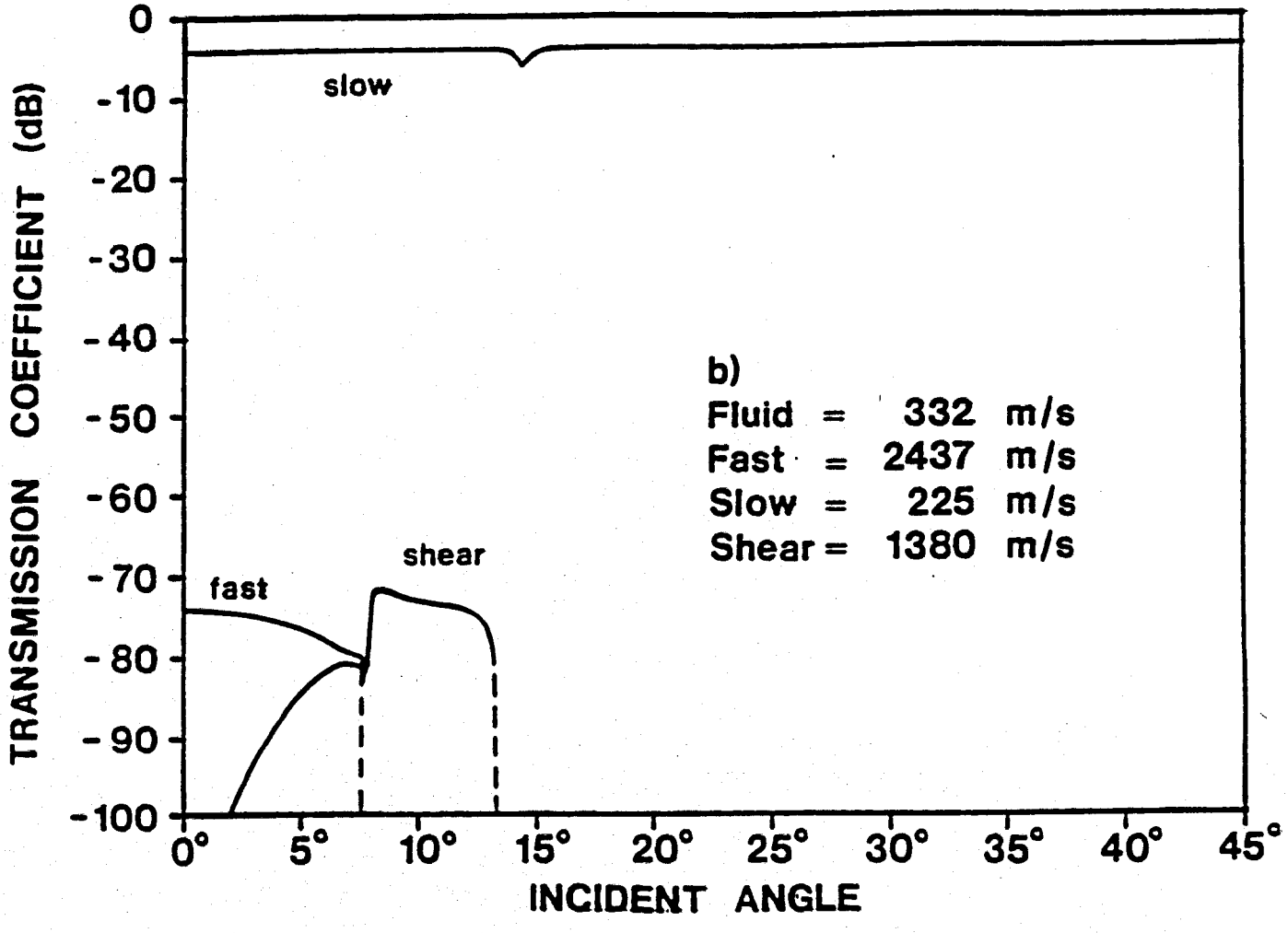

Fig. 30(b). Slow, fast, and shear wave transmission coefficients through air-saturated glass bead specimens.

a_p and simultaneously the wavelength λ be larger than the grain size a_g, as required by the Biot theory [6].

$$\sigma = (2\eta/\rho_f\omega)^{1/2} << a_p << a_g \qquad (11)$$

and

$$a_g k = a_g \omega/c \leq 1, \qquad (12)$$

where η is the viscosity, ρ_f is the fluid density, ω is the angular frequency, and k and c are the wave number and sound velocity of the slow wave, respectively. The slow wave velocity at high frequencies can be easily calculated by assuming a perfectly stiff frame as $c = c_f/\alpha^{1/2}$, while the tortuosity α can be estimated from the porosity ϕ as $\alpha = 1/2(\phi^{-1} + 1)$ [18]. Table II summarizes the relevant physical paramters of water and air as well as f_{min} and f_{max}, i.e. the limits of the frequency window where slow wave propagation is expected (a_g = 200 μm grain diameter and ϕ = 30% porosity was assumed in the calculations). As for determining f_{min} from Eq. 11, we assumed that the pore size is approximately 15% of the grain size, and a_p should be at least four times higher than the viscous skin depth to account for smaller cross-sections at the crucial pore throats.

$$f_{min} = \eta_k/\pi(0.04\ a_g)^2 \qquad (13)$$

and

$$f_{max} = c/2\pi a_g, \qquad (14)$$

where $\eta_k = \eta/\rho_f$.

TABLE II. Physical parameters of water and air at 20° C.

	ρ_f [kg/m^3]	c_f [m/s]	η_k [mm^2/s]	f_{min} [KHz]	f_{max} [KHz]
Water	1000	1480	1	5	810
Air	1.3	332	15	75	180

Table II clearly demonstrates the greatly reduced frequency window where dispersion-free and (more-or-less) attenuation-free slow wave propagation can be expected in air-filled samples of approximately 200 μm grain size. On the other hand, these results do not exclude slow wave propagation in a more general sense over a much larger frequency range. They simply mean that the slow wave becomes increasingly dispersive below 100 KHz and very strong attenuation can be expected above 200 KHz. Naturally, the higher attenuation does not necessarily cause serious problems in detecting the slow wave, since, as we showed earlier, there is not other mechanism for sound propagation.

4.3 EXPERIMENTAL ARRANGEMENT AND RESULTS

Figure 31 shows the block diagram of the experimental arrangement used in this preliminary study to investigate slow wave propagation in air-filled porous specimens. Standard ultrasonic NDE equipment was used without any particular effort to obtain high generation or detection sensitivity. The rather poor coupling between the applied contact transducers resulted in a low, but fairly constant sensitivity over a wide frequency range of 30-500 KHz. In order to assure an acceptable signal-to-noise ratio, extensive signal averaging was used up to 10^5 samples.

Figures 32 and 33 show the reference (without the sample) and transmitted (with the sample at normal incidence) ultrasonic signals for a 1.73 mm thick sintered glass bead sample at 150 KHz and 500 KHz, respectively. The grain diameter was 120 m and the porosity was approximately 30%. Great attention was paid to verifying that the sole mechanism of ultrasonic transmission was the slow compressional mode in the porous sample. We found that the easiest way to do this was to wet the specimen with a few drops of water, which completely killed the transmitted signal in each case. In a few minutes the water usually evaporated and the slow wave reappeared, testifying to the ease of saturating most samples by air.

The reduced sound velocity in the sample can be calculated from the thickness d and the additional time delay T observed upon inserting the specimen between the transducers

$$c = 1/(1/c_f + T/d). \qquad (15)$$

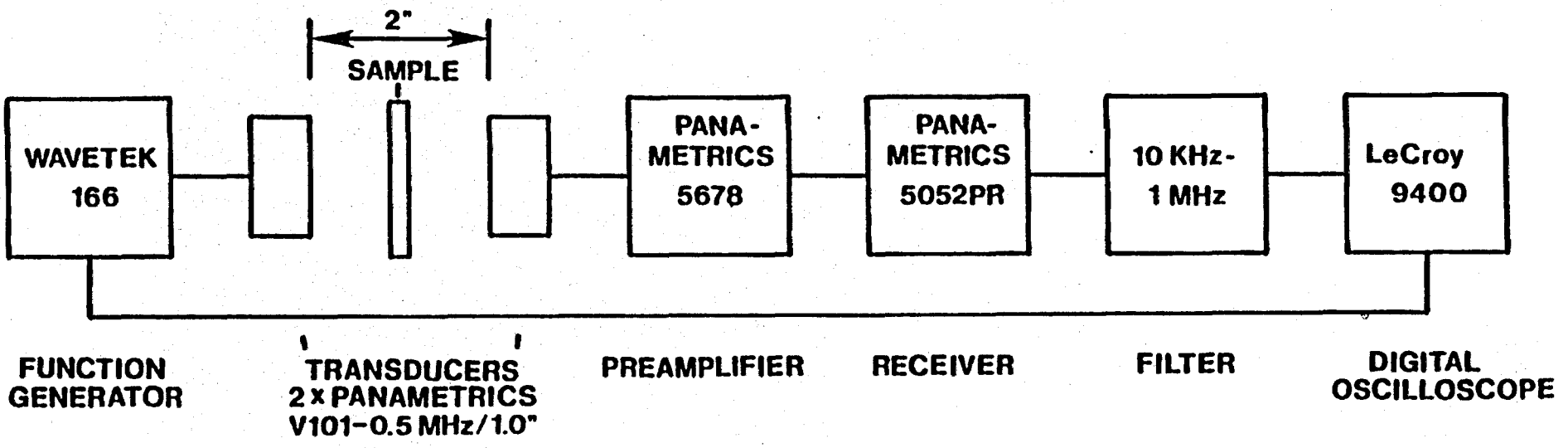

Fig. 31. Block diagram of the experimental arrangement to study slow wave propagation in air-filled porous materials.

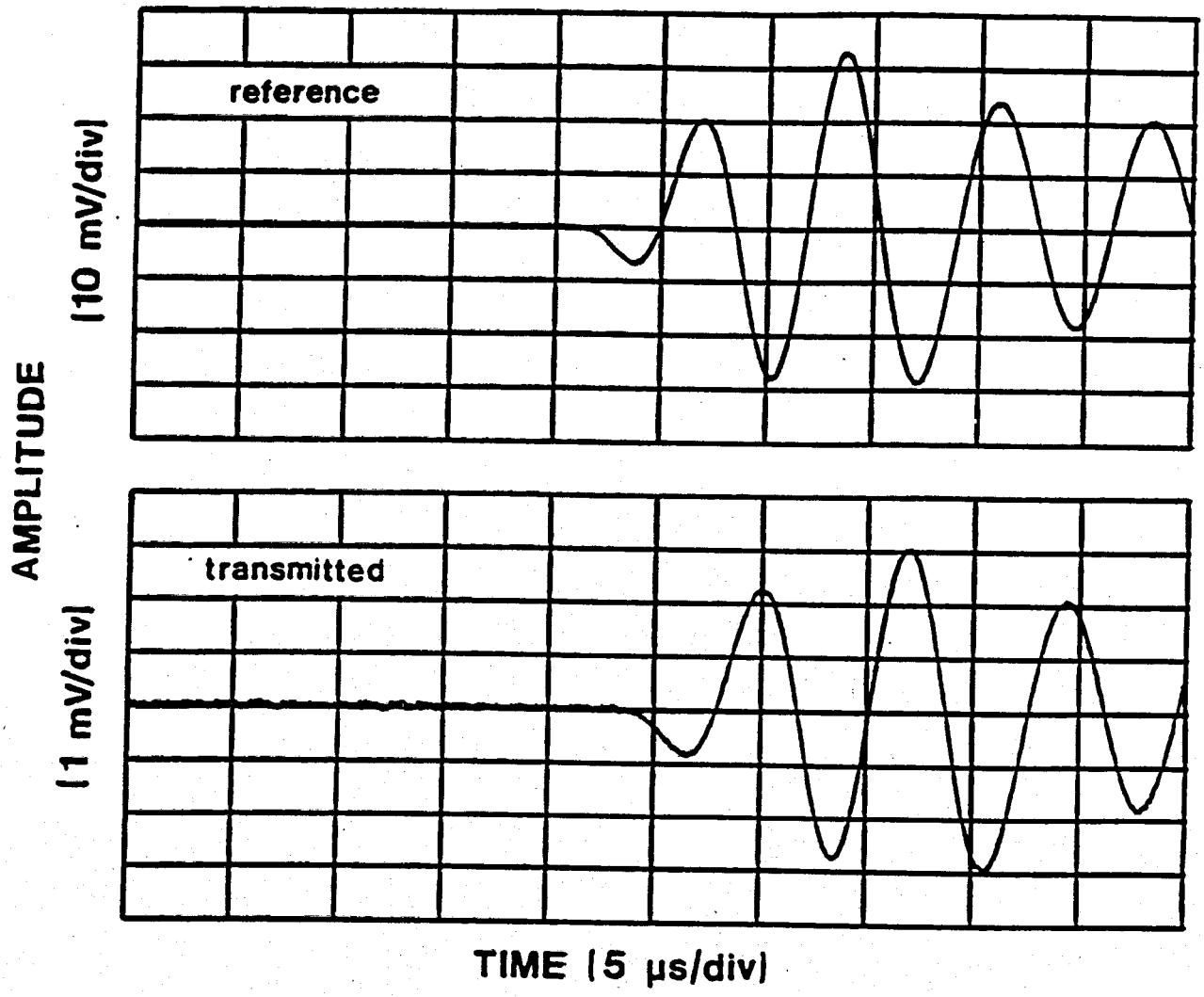

Fig. 32. Reference and transmitted signals through a 1.73 mm thick sintered glass bead sample of 120 μm grain size at 150 KHz.

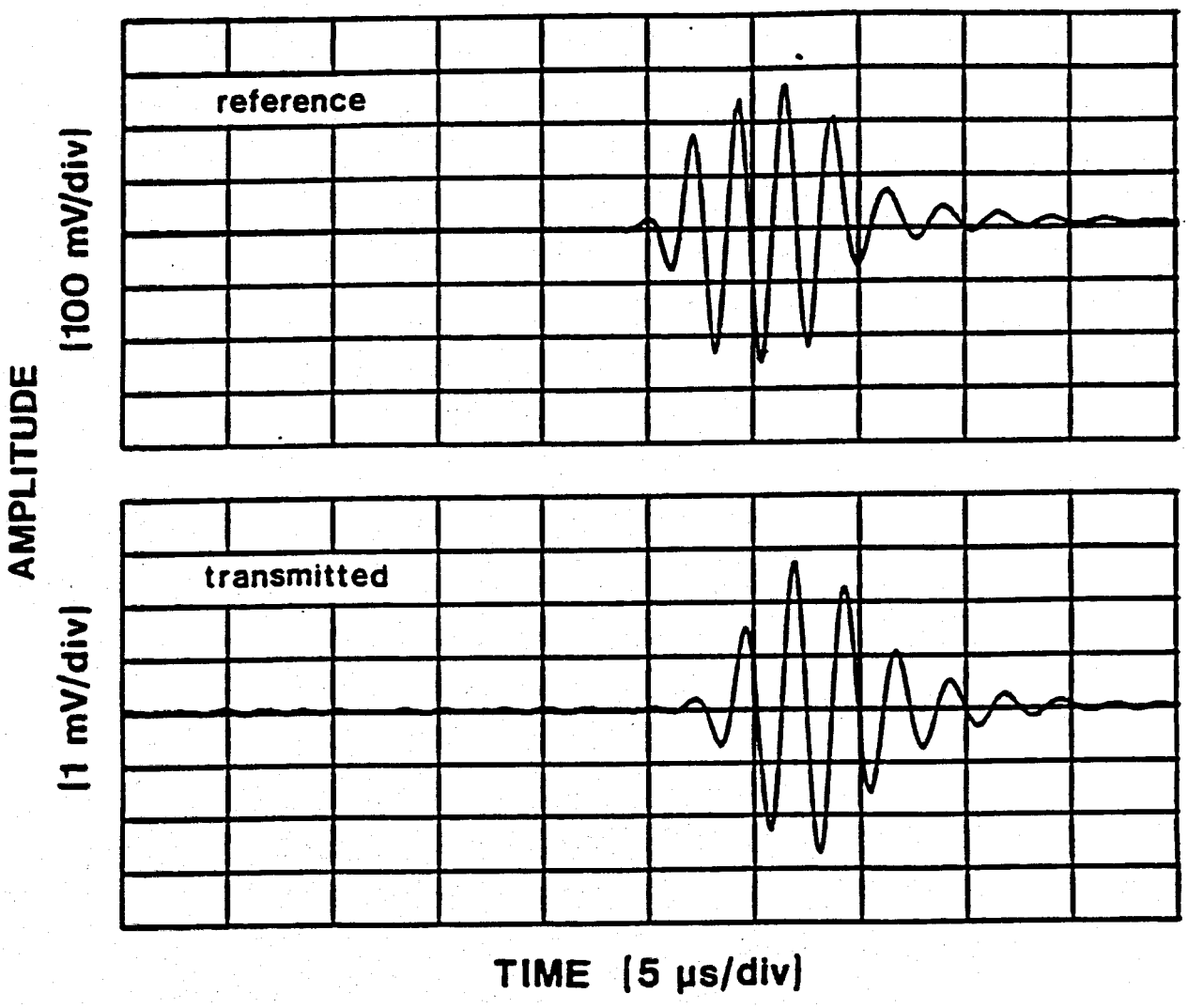

Fig. 33. Reference and transmitted signals through a 1.73 mm thick sintered glass bead sample of 120 μm grain size at 500 KHz.

It should be mentioned that tilting the sample results in an additional backward shift of the detected signal, which can be used to further verify the slow wave nature of the transmitted signal. Continuously changing the angle of incidence is an essential part of Plona's technique to distinguish the slow wave signal from other direct and multiple-reflected signals. In the case of air-saturated samples, normal incidence seems to be the best choice since there are no other signals to eliminate or distinguish from. Furthermore, normal incidence assures the smallest attenuation as well as the most accurate measurement and simplest evaluation.

Figure 34 shows the slow wave velocity as a function of frequency in a sintered glass bead sample of 120 μm grain diameter. From Eq. 13, f_{min} = 200 KHz and at lower frequencies the slow wave exhibits strong dispersion with decreasing velocity. This behavior is in good agreement with the predictions of Biot's theory (see Fig. 12 in Ref. 5b), although quantitative comparison has not been attempted. At higher frequencies there is no apparent dispersion and the slow wave velocity approaches 220 m/s, also in good agreement with the $c_f/\alpha^{1/2}$ = 225 m/s asymptotic value calculated for α = 2.17 tortuosity.

Figure 35 shows the insertion loss (total attenuation) of the transmitted signal as a function of frequency in the same sintered glass bead sample. The measured attenuation seems to be a fairly linear function of frequency over the very wide frequency range of 30-500 KHz. This slope is considerably higher than the $f_{1/2}$ asymptotic dependence predicted by Biot's theory for the $f >> f_{min}$

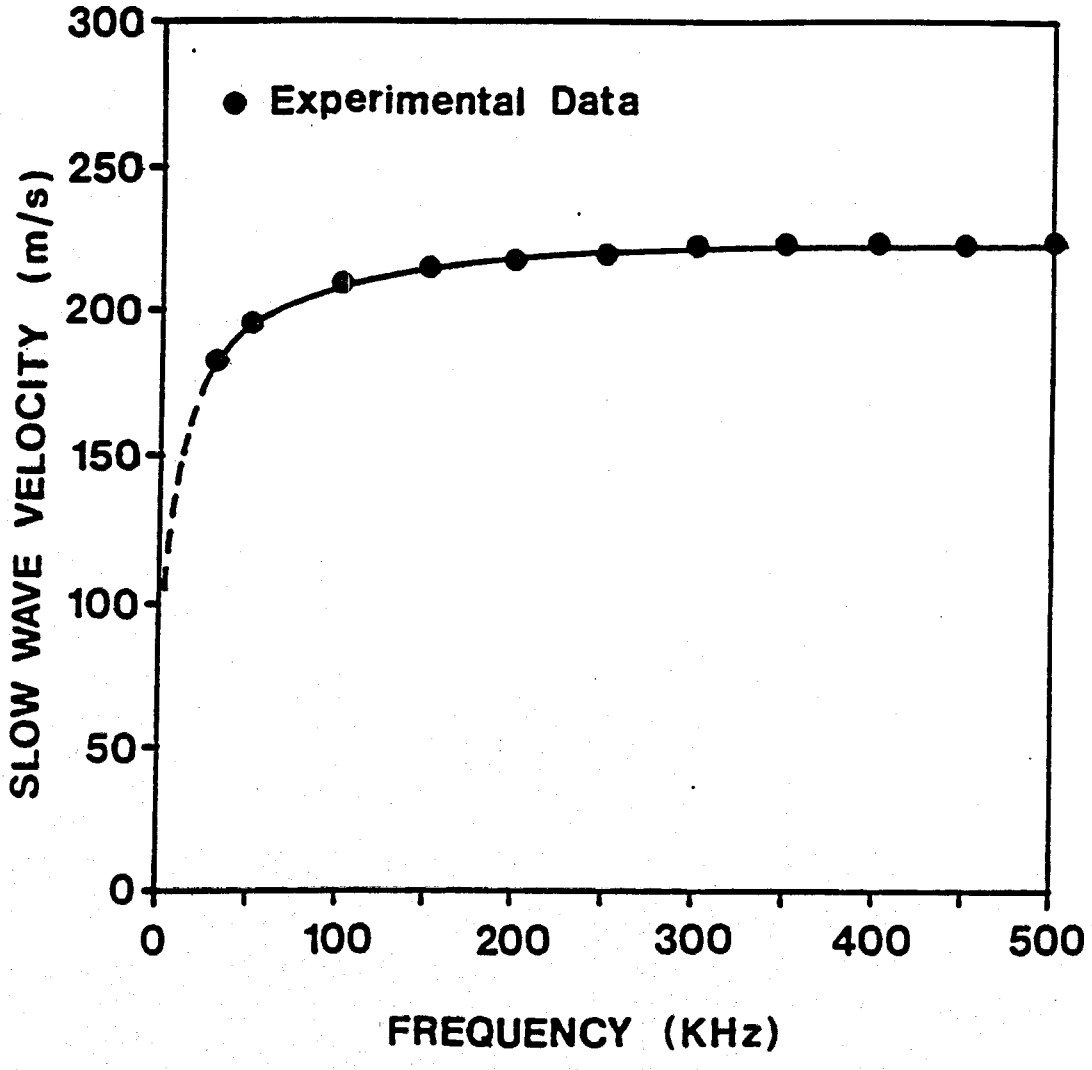

Fig. 34. Slow wave velocity as a function of frequency in a sintered glass bead sample of 120 μm grain size.

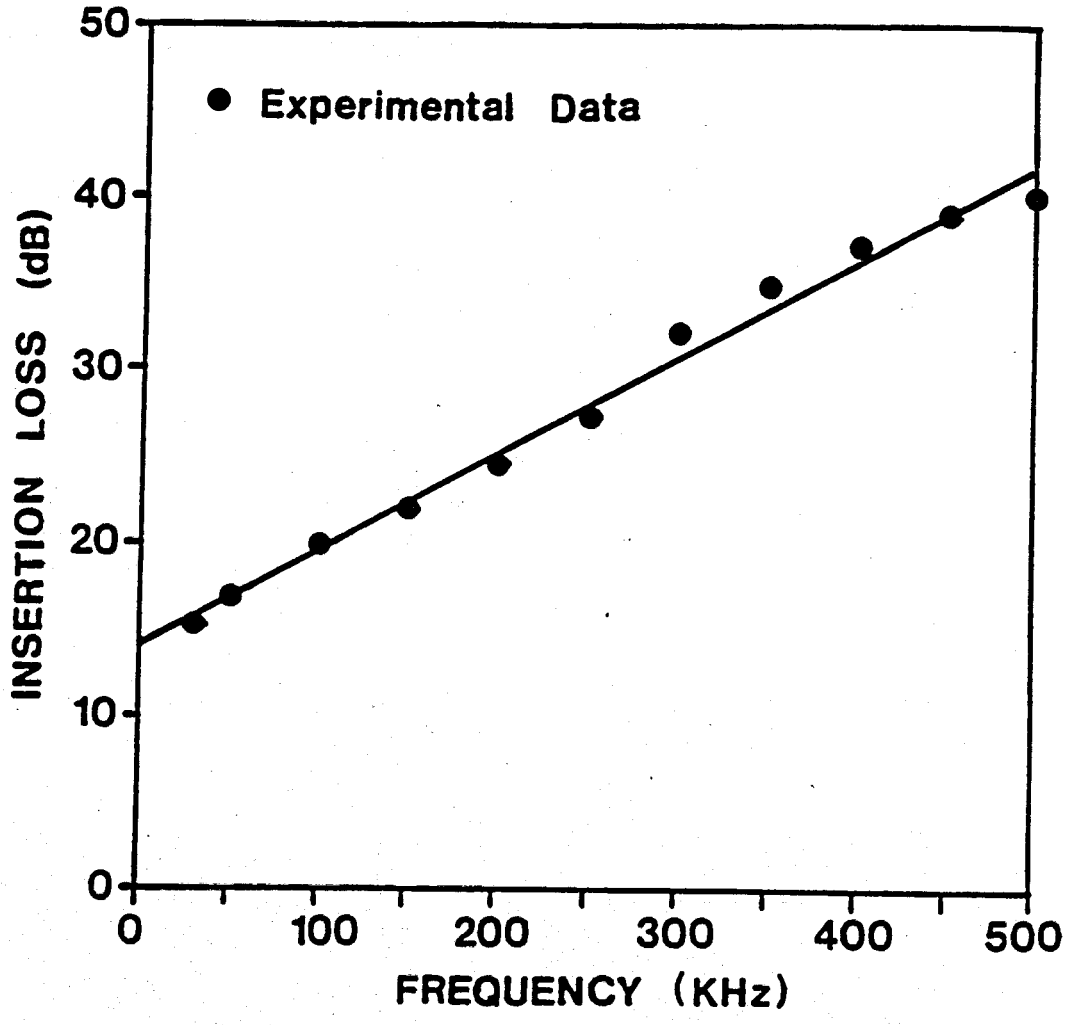

Fig. 35. Insertion loss as a function of frequency in a sintered glass bead sample of 120 μm grain size and 1.73 mm thickness.

frequency range which is most often used with water-saturated samples. However, for air-saturated samples the f/f_{min} ratio is necessarily much lower and the measured frequency dependence of the slow wave is in much better qualitative agreement with Biot's numerical predictions for finite frequencies (see Fig. 14 in Ref. 6b). It should be mentioned that similar behavior, that is more-or-less linear frequency dependence of the slow wave attenuation coefficient, can be observed in water-saturated samples as well (see lines B and C in Fig. 4 in Ref. 20). However, it is even more interesting that the viscous losses dominate the total attenuation in the higher part of the frequency range, too. At 500 KHz, the $a_g k$ product is already 1.7, but there is no sign of sharply increasing attenuation due to scattering. This seems to be partly due to the very high kinematic viscosity of air, which makes the viscous losses dominate over the scattering effect even at relatively high frequencies. Another contribution can be the greatly reduced scattering of the slow compressional mode in air-filled samples where the rigid frame acts like a waveguide. Since there is no appreciable coupling to any other modes of wave propagation, the sound energy cannot help following the tortuous path allowed by the frame and the scattering induced attenuation must be fairly low. This interesting behavior of slow wave attenuation in air-saturated porous specimens needs to be further investigated, too.

One of the main advantages of air saturation over the more conventional technique of water saturation is that slow waves can

be observed without any interference from other bulk modes. As a result, in spite of the inherently higher attenuation, the detection threshold is usually much lower and slow wave propagation can be readily observed in natural rocks as well. This is a unique feature of the air saturation technique since slow wave propagation has never been observed in water-saturated natural rocks. Figure 36 shows the reference and transmitted signals through a 2 mm thick brown Berea sandstone sample of 600 mdarcy permeability. As another example, Fig. 37 shows the reference and transmitted signals through a 1 mm thick gray Berea sandstone sample of 400 mdarcy permeability. In both cases, the slow wave nature of the transmitted signal was readily verified by a few drops of water which completely eliminated the transmitted signal by blocking the free airflow through the open pores in the rock. The principal geometrical and acoustical parameters of these rocks and the sintered glass bead sample are summarized in Table III. The slow wave velocity and attenuation were measured at 150 KHz and the tortuosity was calculated as $\alpha \approx c_f^2/c^2$.

TABLE III. Physical parameters of different porous samples.

	Sintered Glass Bead	Brown Berea Sandstone	Gray Berea Sandstone
Thickness [mm]	1.73	2.0	1.0
Grain Size [μm]	120	~400	~200
Permeability [mdarcy]	6000	600	400
Slow Wave Velocity [m/s]	215	190	164
Tortuosity	2.3	3.0	4.0
Attenuation [dB]	22	46	52

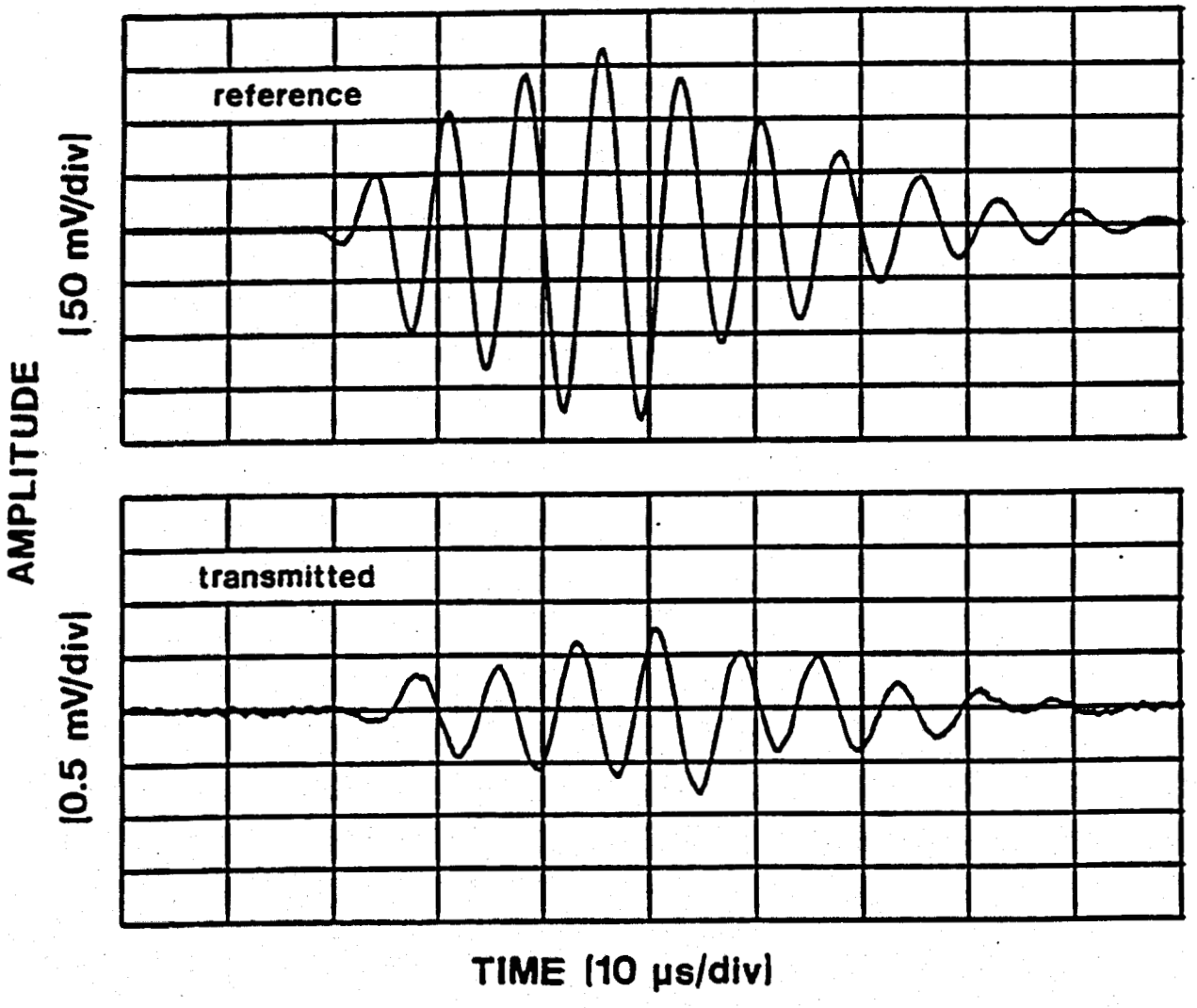

Fig. 36. Reference and transmitted signals through a 2 mm thick brown Berea sandstone sample at 150 KHz.

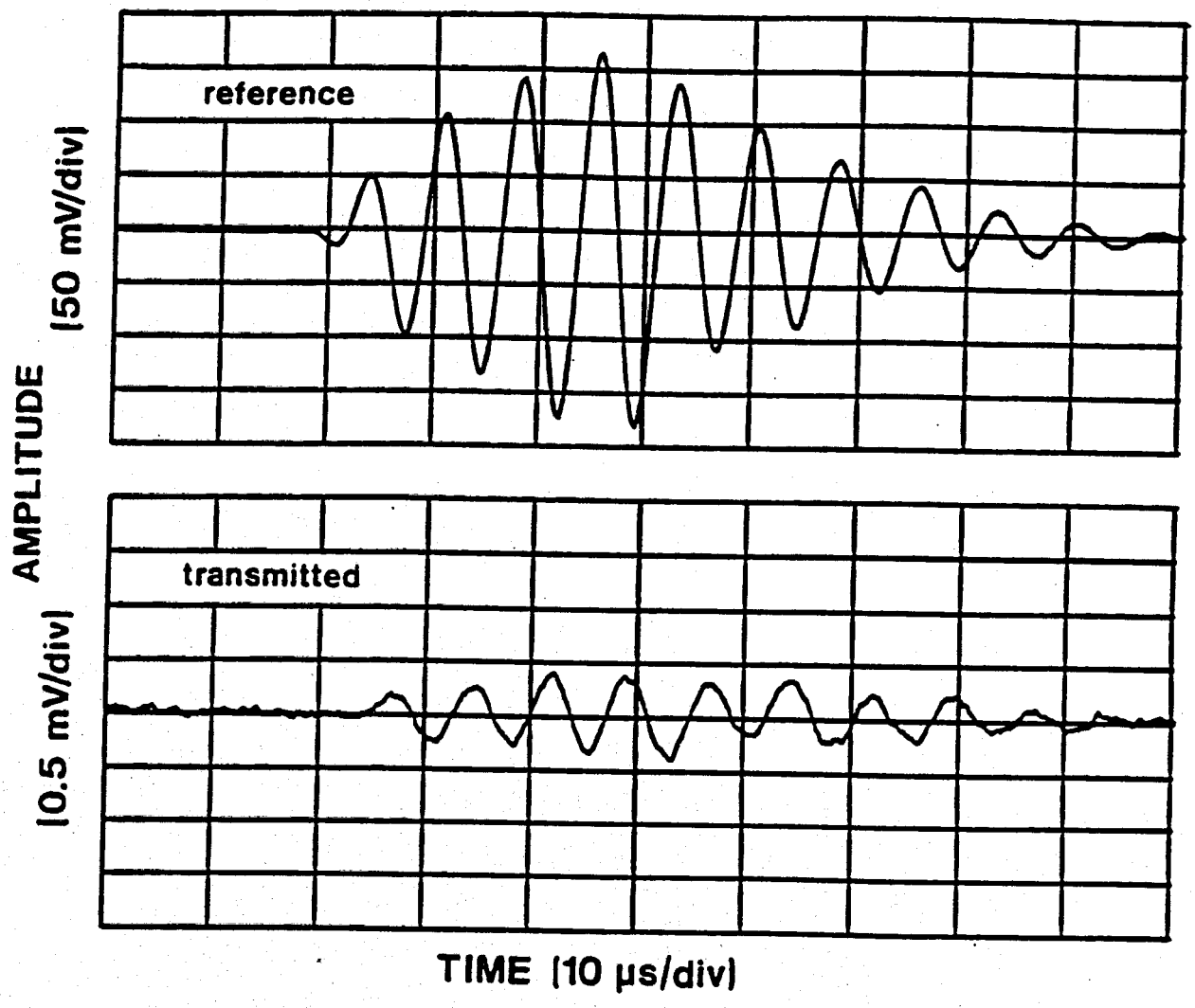

Fig. 37. Reference and transmitted signals through a 1 mm thick gray Berea sandstone sample at 150 KHz.

II. PROPOSED RESEARCH

Objectives of Proposed Research

During the next three years of this proposed work we plan to continue our investigation of ultrasonic waves, especially the slow compressional wave, with fluid-saturated porous solids, especially rocks. This research effort should find applications in the geophysical evaluation of fluid-bearing porous rocks where parameters such as tortuosity, permeability, saturation level, and internal impurities are difficult to measure by conventional techniques.

Summary of Proposed Research

The proposed investigation of ultrasonic wave interaction with fluid-saturated porous materials may be divided into three major subtasks:

1. Experimental study of surface wave propagation on fluid-saturated porous materials. A new, so-called direct excitation technique will be used on both air- and water-saturated samples.
2. Further development of the Lamb wave technique recently introduced to study guided wave propagation in thin fluid-saturated porous plates. The analytical treatment will be extended to account for viscous losses and scattering inhomogeneities.
3. Theoretical and experimental study of slow wave propagation in fluid-saturated natural rocks. A new

technique based on the transmission of airborne ultrasound through air-saturated porous plates will be used to determine otherwise inaccessible material properties such as tortuosity, permeability, internal friction caused by impurities, etc.

1 SURFACE WAVE TECHNIQUE

Generally, two types of interface modes can propagate along the surface of a solid sample immersed in fluid: there is a true mode called Stoneley wave and a pseudo-mode called leaky Rayleigh wave. For fluid-saturated porous solids there are three changes in this simple surface mode structure. First, in many cases, the shear velocity of the fluid-saturated material is lower than the sound velocity in the fluid, and the leaky Rayleigh mode becomes nonpropagatory. It should be mentioned that in natural rocks the shear velocity of the saturated sample is somewhat lower than that of the dry skeleton [21], and that this difference might be responsible for the disappearance of the expected Rayleigh mode. Second, the normally true Stoneley mode might become leaky into the slow compressional wave causing very strong attenuation. Finally, a new true surface mode can appear with phase velocity lower than that of all the other modes if the pores on the surface of the specimen are closed [1].

This third mode offers an excellent possibility to study the surface conditions of a porous sample. It should be mentioned that a somewhat less obvious change in the Stoneley mode can also be used to evaluate the surface quality. In samples of moderate frame stiffness, the Stoneley mode approaches either the shear or the considerably lower Rayleigh velocity depending on whether the pores are closed or open [1]. Since the suggested direct excitation technique is much more accurate than the formerly used corrugated surface method, this difference can be readily revealed. Actually, this new technique generates a shear-type bulk wave and a Rayleigh

or Stoneley-type interface wave simultaneously, therefore very small velocity differences can be detected. Even when the principal pulses are not sufficiently separated to resolve them in the time domain, their relative delay can be measured from the periodic frequency modulation observed in the spectrum of the overall signal due to alternating constructive and destructive interference between them. Of course, the interface wave velocity can then be easily calculated from the measured time difference and the known value of the shear velocity [5].

(For further background, see Section 1 of Progress Report.)

2 LAMB WAVE TECHNIQUE

The main thrust of our former research effort was directed at finding indications of slow wave propagation in natural rocks, which offers a unique acoustical means to evaluate otherwise inaccessible material properties such as tortuosity and permeability. Recently, Klimenatos and McCann showed that the disappearance of the slow wave is probably due to internal impurities, such as submicron clay perticles, found in all types of natural rocks [13]. Such clay particles deposited both within the pore throats and on the surfaces of the rock grains greatly increase viscous drag between the fluid and the solid frame, which results in excessive attenuation and complete disappearance of the slow wave.

In order to increase the detectability of the slow compressional wave in such highly attenuating materials, we have to simultaneously reduce the sample thickness and the ultrasonic frequency. In this case, the acoustic wave-material interaction cannot be described in the simple terms of bulk modes anymore. Rather, Lamb modes of a thin fluid-saturated porous plate should be considered in order to determine the elastic properties of the plate from the numerous resonances produced at different incident angles. We found that the lowest extensional mode of a fluid-saturated porous plate is due to the slow wave component and it has a cut-off frequency of $fd = C_{slow}/2$. This frequency times thickness product can be regarded as the lowest limit where slow wave propagation can be observed separately from other bulk modes.

The Lamb wave technique was found to be of superior sensitivity with respect to the more conventional bulk technique using relatively thick plates. Still, experiments with natural rock specimens clearly indicated that viscous losses can be extremely high even for this lowest extensional mode. In order to account for such losses in the theoretical calculations, we are going to introduce appropriate changes in our analytical model. Parametric studies will be carried out to find the optimal detection conditions for weak slow compressional waves in thin plates of natural rocks.

In a further effort to observe slow wave propagation in water-saturated rocks, we are going to apply different chemical and mechanical cleaning techniques to remove an increasing portion of the internal impurities commonly found in natural rocks. This part of the work will be done in close cooperation with Brian Bonner of the Lawrence Livermore National Laboratory. Acoustic measurements will be made in different phases of the gradual cleaning process and the results will be compared to data obtained by the air-saturation technique to be described in the next chapter.

(For further background, see Section 3 of Progress Report.)

3 AIR-SATURATION TECHNIQUE

Recently, we developed a new technique based on the transmission of airborne ultrasonic waves through air-saturated porous plates in order to observe weak slow compressional waves in natural rocks. To the best of our knowledge, our preliminary results represent the first irrefutable evidence of slow wave propagation in air-saturated natural rocks, such as different types of sandstones. We are going to further develop this technique to increase the sensitivity so that a wide range of porous rocks can be studied without any particular limitations on porosity, tortuosity, level of internal impurities, sample thickness, etc. Furthermore, increased sensitivity will make it possible to use higher frequencies where the slow wave is more-or-less dispersion-free and the crucial tortuosity parameter can be directly calculated from the measured slow wave velocity.

We have also demonstrated that the proposed air-saturation technique makes it possible to observe and study the slow compressional wave throughout the transition from the low-frequency dispersive region to the high-frequency dispersion-free range. In an air-filled porous sample, coupling between the low-density fluid and the much stiffer frame is mainly due to viscous forces. An analytical technique will be developed from the general theory of Biot to calculate the frequency-dependent slow wave velocity and attenuation coefficient as a function of fluid viscosity, frame tortuosity, and an additional factor to be introduced to describe the increased viscous drag caused by internal impurities. It is expected that this analytical technique will lead to the solution

of the inverse problem, too, i.e. tortuosity and the degree of internal impurity can be detemined from the measured slow wave velocity and attenuation, respectively.

Special attention will be paid to the unique attenuation mechanism observed in air-filled porous specimens. A new theoretical model will be developed to describe the greatly reduced scattering induced attenuation of the slow compressional wave. Since the frame acts like a rigid waveguide and mode-conversion to other wave modes is negligible, the principal attenuation mechanism turns out to be the random phase cancellation between slow wave components following separate, slightly different tortuous paths within the porous plate rather than the loss of scattered energy responsible for high attenuation in water-saturated samples. This diffuse propagation of the slow compressional wave through an air-filled porous plate will be modeled by the random phase perturbation technique previously introduced to assess scattering induced attenuation of ultrasonic waves transmitted through a rough interface [22].

(For further background, see Section 4 of Progress Report.)

REFERENCES

1. S. Feng and D.L. Johnson, J. Acoust. Soc. Am. 74, 906 (1983); 74, 915 (1983).

2. A. Jungman, L. Adler, and G. Quentin, J. Appl. Phys. 53, 4673 (1982).

3. A. Jungman, L. Adler, J.D. Achenbach, and R. Roberts, J. Acoust. Soc. Am. 74, 1025 (1983).

4. M.J. Mayes, P.B. Nagy, L. Adler, B.P. Bonner, and R. Streit, J. Acoust. Soc. Am. 79, 249 (1986).

5. P.B. Nagy and L. Adler, J. Acoust. Soc. Am. 86, S94 (1989).

6. M.A. Biot, J. Acoust. Soc. Am. 28, 168 (1956); 28, 179 (1956).

7. T.J. Plona, Appl. Phys. Lett. 36, 259 (1980).

8. J. Geerstma and D.G. Smit, Geophys. 26, 169 (1961).

9. H. Deresiewicz and J.T. Rice, Bull. Seismol. Soc. Am. 50, 599 (1960); 54, 409 (1964).

10. R.D. Stoll and T. Kan, J. Acoust. Soc. Am. 70, 149 (1981).

11. L. Adler, K. Wu, and Q. Xue, Ultrason. Internat. '89, 1013 (1989).

12. D.L. Johnson and T.J. Plona, J. Acoust. Soc. Am. 72, 556 (1982).

13. T. Klimentos and C. McCann, Geophys. 53, 1605 (1988).

14. Lord Rayleigh, Proc. London Math. Soc. 20, 225 (1889).

15. H. Lamb, Proc. Roy. Soc. (London), A 93, 114 (1917).

16. L.E. Pitts, T.J. Plona, and W.G. Mayer, J. Acoust. Soc. Am. 60(2), 374 (1976).

17. A. Jungman, G. Quentin, L. Adler, and Q. Xue, J. Appl. Phys. 66, 5179 (1989).

18. J.G. Berryman, Appl. Phys. Lett. 37, 382 (1980).

19. R.C. Weast, Handbook of Chemistry and Physics, 51st ed., The Chemical Rubber Co. (1970).

20. T.J. Plona and K.W. Winkler, in Multiple Scattering of Waves in Random Media and Random Surfaces, (Pennsylvania State University, 1985) pp. 341-356.

21. T. Bourbie, A. Coussy, and B. Zinszner, Acoustics of Porous Media, (Gulf Publishing Co., Houston, 1987).

22. P.B. Nagy and L. Adler, J. Acoust. Soc. Am. 82, 193 (1987).

PUBLICATIONS

1. P.B. Nagy, L. Adler, K. Lewis, and B. Bonner, "Ultrasonic NDE of Fluid-Saturated Porous Solids," ASNT Characterization of Materials and Flaws Spring Conference (1988).

2. A. Jungman, L. Adler, and G. Quentin, "Ultrasonic Velocity Measurements in Porous Materials," in Nondestructive Characterization of Materials (Springer-Verlag, Berlin, 1989) pp. 122.

3. Q. Xue, K. Wu, L. Adler, A. Jungman, and G. Quentin, "Generalized Lamb Modes in Fluid-Saturated Porous Plate," in Review of Progress in Quantitative NDE (Plenum Press, New York, 1989), Vol. 8A, pp. 21.

4. A. Jungman, G. Quentin, Q. Xue, and L. Adler, "Ultrasonic Wave Interaction with Fluid-Saturated Porous Plates," Proc. 13th Internat. Cong. on Acoustics, Vol. 1, 313 (1989).

5. L. Adler, K. Wu, and Q. Xue, "Ultrasonic Wave Mode Conversion in Fluid-Saturated Porous Materials," Ultrason. Internat. '89, 1013 (1989).

6. L. Adler, P.B. Nagy, and Q. Xue, "A Study of Surface Waves and Lamb Waves in Fluid-Saturated Porous Materials," Proc. II Internat. Symp. on Surface Waves in Solids and Layered Structures (1989).

7. A. Jungman, G. Quentin, L. Adler, and Q. Xue, "Elastic Property Measurements in Fluid-Filled Porous Materials," J. Appl. Phys. 66, S179 (1989).

8. K. Wu, Q. Xue, and L. Adler, "Reflection and Transmission of Elastic Waves from a Fluid/Porous Solid Interface," J. Acoust. Soc. Am. 85, S93 (1989).

9. L. Adler, P.B. Nagy, and Q. Xue, "Ultrasonic Surface Waves and Lamb Waves in Fluid-Saturated Porous Solids," To be published Proc. IEEE Ultrason. Symp. (1989).

10. Q. Xue and L. Adler, "An Improved Method to Measure Slow Compressional Wave in Fluid-Saturated Porous Plates by Using Lamb Modes," To be published in Review of Progress in Quantitative NDE, Vol. 9 (1990).

11. K. Wu, Q. Xue, and L. Adler, "Reflection and Transmission of Elastic Waves from a Fluid-Saturated Porous Solid Boundary," submitted for publication to the J. Acoust. Soc. Am. (1989).

12. K. Wu, Q. Xue, and L. Adler, "Elastic Wave Interaction at the Boundary Between Two Fluid-Filled Porous Materials," submitted for publication to the J. Acoust. Soc. Am. (1989).

PERSONNEL

The proposed research will be directed by Dr. Laszlo Adler, Taine McDougal Professor of Welding Engineering and Engineering Mechanics and Director, NDE Program, who has done extensive research on ultrasonic materials characterization and nondestructive evaluation for over 25 years. He has over 150 publications.

Dr. Peter B. Nagy, Research Scientist, will be the Co-Investigator. Dr. Nagy has over 15 years experience in ultrasonic NDE and optics. He has over 50 publications.

One Ph.D. student will participate in the proposed research.

CURRENT FEDERAL SUPPORT

Laszlo Adler - Principal Investigator

Support Source: Air Force Materials Research Lab through Iowa State University/Ames Laboratory
Project Title: Ultrasonic Detection of Porosity in Aluminum Casts
Award Amount: $35,800
Period Covered: 10/01/89 - 09/30/90

Support Source: Department of Energy, Division of Materials Sciences
Project Title: Investigations of Ultrasonic Wave Interactions at Imperfect Boundaries Separating Anisotropic Materials
Award Amount: $94,700
Period Covered: 03/31/90 - 03/30/91

Support Source: Office of Naval Research
Project Title: Novel Ultrasonic Techniques for Interface Studies
Award Amount: $25,000
Period Covered: 12/01/89 - 06/30/90